THE FORM OF LATERAL VISCOSITY IN ATMOSPHERIC FLOWS

Orlin Robert Scrivener

NAVAL POSTGRADUATE SCHOOL
Monterey, California

THESIS

The Form of Lateral Viscosity

in Atmospheric Flows

by

Orlin Robert Scrivener

Thesis Advisor: G. J. Haltiner

September 1972

The Form of Lateral Viscosity

in Atmospheric Flows

by

Orlin Robert Scrivener
Lieutenant, United States Navy
B.S., United States Naval Academy, 1966

Submitted in partial fulfillment of the
requirements for the degree of

MASTER OF SCIENCE IN METEOROLOGY

from the

NAVAL POSTGRADUATE SCHOOL
September 1972

ABSTRACT

Long term numerical integrations were performed on a two-dimensional model utilizing the barotropic vorticity equation including a space-and time-dependent forcing function and a laminar-type viscosity term. Three different forms of the laminar type viscosity or dissipation term were used. A comparison was made of the effects these different dissipation terms had on the time-dependence of total kinetic energy, total enstrophy, and total gradient of vorticity squared, the spectral distribution of kinetic energy and enstrophy, and the stream function field. A difference of behavior of all the above variables was found for each form of dissipation.

TABLE OF CONTENTS

I. INTRODUCTION ---------- 9

II. MATHEMATICAL MODEL ---------- 11

III. FORMS OF DISSIPATION ---------- 13

IV. DISCUSSION OF RESULTS ---------- 15

V. CONCLUSIONS ---------- 20

APPENDIX A - COMPLETE DESCRIPTION OF THE MODEL ------ 23

APPENDIX B - FINITE DIFFERENCE EQUATIONS ---------- 25

APPENDIX C - RELAXATION TECHNIQUE ---------- 27

APPENDIX D - TIME STEP SCHEMES ---------- 29

LIST OF REFERENCES ---------- 62

INITIAL DISTRIBUTION LIST ---------- 63

FORM DD 1473 ---------- 65

LIST OF FIGURES

1. Grid for the model ---------- 23

2. Total kinetic energy vs. time for the zero forcing and zero dissipation case and for A = constant form of dissipation ---------- 30

3. Total kinetic energy vs. time for the A_S form of dissipation with gamma = .5, .2, and .13----- 31

4. Total kinetic energy vs. time for the A_L form of dissipation with gamma = .5 and .2 ---------- 32

5. Total enstrophy vs. time for the zero forcing and zero dissipation case and for A = constant form of dissipation ---------- 33

6. Total enstrophy vs. time for the A_S form of dissipation with gamma = .5, .2, and .13-------- 34

7. Total enstrophy vs. time for the A_L form of dissipation with gamma = .5 and .2---------- 35

8. Total gradient of vorticity squared vs. time for the zero forcing and zero dissipation case and for A=constant form of dissipation----- 36

9. Total gradient of vorticity squared vs. time for the A_S form of dissipation with gamma = .5, .2, and .13 ---------- 37

10. Total gradient of vorticity squared vs. time for the A_L form of dissipation with gamma = .5 and .2---------- 38

11. Initial spectral distribution of kinetic energy and enstrophy ---------- 39

12. Spectral distribution of kinetic energy and enstrophy at mid-time and end-time for the zero dissipation and zero forcing case------ 40

13. Spectral distribution of kinetic energy and enstrophy at mid-time and end-time for the A = constant form of dissipation ---------- 41

14. Spectral distribution of kinetic energy and enstrophy at mid-time and end-time for the A_S form of dissipation with gamma = .5------ 42

15. Spectral distribution of kinetic energy and enstrophy at mid-time and end-time for the A_S form of dissipation with gamma = .2 --------- 43

16. Spectral distribution of kinetic energy and enstrophy at mid-time and end-time for the A_S form of dissipation with gamma = .13--------- 44

17. Spectral distribution of kinetic energy and enstrophy at mid-time and end-time for the A_L form of dissipation with gamma = .5 --------- 45

18. Spectral distribution of kinetic energy and enstrophy at mid-time and end-time for the A_L form of dissipation with gamma = .2 --------- 46

19. Initial stream function field ---------- 47

20. Stream function field at 5 days for zero forcing and zero dissipation case ---------- 48

21. Stream function field at 5 days for A = constant form of dissipation ---------- 48

22. Stream function field at 10 days for zero forcing and zero dissipation case ---------- 49

23. Stream function field at 10 days for A = constant form of dissipation ---------- 49

24. Stream function field at 15 days for zero forcing and zero dissipation case ---------- 50

25. Stream function field at 15 days for A = constant form of dissipation ---------- 50

26. Stream function field at 20 days for zero forcing and zero dissipation case ---------- 51

27. Stream function field at 20 days for A = constant form of dissipation ---------- 51

28. Stream function field at 5 days for A_L form of dissipation with gamma = .5 ---------- 52

29. Stream function field at 5 days for A_L form of dissipation with gamma = .2 ---------- 52

30. Stream function field at 10 days for A_L form of dissipation with gamma = .5 ---------- 53

31. Stream function field at 10 days for A_L form of dissipation with gamma = .2 ---------- 53

32. Stream function field at 15 days for A_L form of dissipation with gamma = .5 ---------- 54

33. Stream function field at 15 days for A_L form of dissipation with gamma = .2 ---------- 54

34. Stream function field at 20 days for A_L form of dissipation with gamma = .5 ---------- 55

35. Stream function field at 20 days for A_L form of dissipation with gamma = .2 ---------- 55

36. Stream function field at 5 days for A_S form of dissipation with gamma = .5 ---------- 56

37. Stream function field at 5 days for A_S form of dissipation with gamma = .2 ---------- 56

38. Stream function field at 10 days for A_S form of dissipation with gamma = .5---------- 57

39. Stream function field at 10 days for A_S form of dissipation with gamma = .2 ---------- 57

40. Stream function field at 15 days for A_S form of dissipation with gamma = .5---------- 58

41. Stream function field at 15 days for A_S form of dissipation with gamma = .2 ---------- 58

42. Stream function field at 20 days for A_S form of dissipation with gamma = .5---------- 59

43. Stream function field at 20 days for A_S form of dissipation with gamma = .2---------- 59

44. Stream function field at 5 days for A_S form of dissipation with gamma = .13 ---------- 60

45. Stream function field at 10 days for A_S form of dissipation with gamma = .13 ---------- 60

46. Stream function field at 15 days for A_S form of dissipation with gamma = .13 ---------- 61

47. Stream function field at 20 days for A_S form of dissipation with gamma = .13 ---------- 61

LIST OF SYMBOLS

β	derivative of coriolis parameter at mid-latitude
γ	constant coefficients
ζ	vorticity
ψ	stream function
A	coefficient of "eddy diffusion"
S	source term
t	time
K.E.	kinetic energy
$\frac{\zeta^2}{2}$	enstrophy

ACKNOWLEDGEMENTS

The author wishes to express his deep appreciation and thanks to Dr. George J. Haltiner and Dr. W. L. Gates whose interest, counsel and recommendations were truly exceptional. Dr. Gates made the initial suggestion of the topic.

I would further like to thank Dr. R. L. Haney and Dr. R. T. Williams for their assistance and suggestions which contributed to this study.

I. INTRODUCTION

With modern computers it is possible to simulate turbulent motion in three dimensions. As a consequence of theoretical studies as well as experimental results, the turbulent processes at work in the three-dimensional case are reasonably well understood. In recent years, however, studies have also been conducted on two-dimensional turbulence as an analogue to the large scale motions of the atmosphere. The behavior of the two-dimensional turbulence parameters is just beginning to be discovered.

The principal distinguishing feature of two-dimensional turbulence is the tendency of its energy-containing eddies to grow indefinitely in scale. In any finite difference model of two-dimensional turbulent flow, therefore, the energy transfer between large scales will be computed more or less correctly. At the scale of the grid interval, however, aliasing errors can transfer energy erroneously to all of the larger scales destroying the sense of the calculation. This problem can be alleviated by the removing of energy from scales near the grid scale. The energy thus "dissipated" is that which would cascade to smaller scales in real flow.

A common procedure in numerical modeling is to parameterize the sub-grid scale dissipation in the form of a diffusion process with an assigned coefficient of "eddy

diffusion", A, as in $\nabla \cdot (A\nabla\zeta)$, where ζ is the fluid property being dissipated.

The objective of the present work is to compare the behavior of certain properties generated by different forms of the eddy diffusion term in two-dimensional turbulent flow.

II. THE MATHEMATICAL MODEL

The principal equation of the model is the barotropic vorticity equation including a space- and time-dependent forcing function and a laminar-type viscosity, written as

$$\frac{\partial \zeta}{\partial t} + J(\psi,\zeta) + \beta \frac{\partial \psi}{\partial x} = S + \nabla \cdot (A\nabla\zeta) \qquad (1)$$

The wind velocity is associated with the stream function by the following equation:

$$W = i\frac{\partial \psi}{\partial y} + j\frac{\partial \psi}{\partial x} \qquad (2)$$

The vorticity is the laplacian of the stream function,

$$\nabla^2\psi = \zeta \qquad (3)$$

In all of the numerical experiments undertaken in this study, the regime of integration is taken to be a rectangle with cyclic boundary condition in the x direction and free slip boundary conditions on the northern and southern boundaries. (See Appendix A).

The numerical integration of Equation (1) and (3) was performed by first replacing them with a pair of finite difference equations to be solved for the variables prescribed on a cartesian grid. (See Appendix B).

The numerical space-differencing method used on the nonlinear terms of Equation (1) is the second-order scheme developed by Arakawa (1966) which conserves kinetic energy and enstrophy within the nonlinear terms. The laplacians in Equations (1) and (3) were approximated by the methods

discussed in Appendix B. Time integration was performed by the explicit centered leapfrog scheme, except for the first step and restarts every 50 time steps by the iterative Euler-backward scheme. (See Appendix D).

The forcing function S used in these experiments was a crude approximation for the baroclinic driving forces in the atmosphere. S was negatively related to the stream function and was scaled to the magnitude of the rate of change of vorticity. (See Appendix A). The source term was set to zero at mid-time in each experiment conducted to study the decay properties of each form of dissipation.

The initial stream field was defined to have components in wave numbers 2, 4, and 6 and of such magnitude as to simulate the 500-mb patterns. (See Appendix A).

The different forms of the dissipation are discussed in the following chapter.

III. FORMS OF DISSIPATION

In Equation (1), the last term on the right hand side represents a laminar-type viscosity or dissipation and is written as $\nabla \cdot (A\nabla\zeta)$. The experiments assumed three different forms of A which represents the coefficient of "eddy diffusion."

In the first form, A was taken to be the constant .5 x 10^6 m^2 sec^{-1}. This value was used to produce an equilibrium solution of a one-wave stream function field within the time frame of these experiments.

The second form of A was taken to be a function of the wind field as formulated by Smagorinsky (1963) for three-dimensional turbulence:

$$A_S = \gamma_1 |D_*| (\Delta x)^2 \qquad (4)$$

where D_* is the deformation on the grid Δx and γ_1 is a constant.

The deformation is defined as:

$$|D_*| = \sqrt{D_T^2 + D_S^2}$$

where

$$D_T = \frac{\partial u}{\partial x} - \frac{\partial v}{\partial y}$$

and

$$D_S = \frac{\partial v}{\partial x} + \frac{\partial u}{\partial y}$$

The third and final form of A was that proposed by Leith (1969) for two-dimensional turbulence, namely,

$$A_L = \gamma_2 \, |\nabla\zeta| \, (\Delta x)^3 \qquad (5)$$

Here γ_2 is a constant and $|\nabla\zeta|$ is the scalar magnitude of the gradient of vorticity.

The finite difference forms of the above equations may be found in Appendix B.

IV. DISCUSSION OF RESULTS

Seven experiments were conducted for comparison and evaluation of the different forms of dissipation as follows:

(1) Equation (1) with the source and dissipation terms removed.

(2) A constant coefficient for A in Equation (1).

(3) Smagorinsky's form of A (Equation 4) with $\gamma_1 = .5$.

(4) Smagorinsky's form of A with $\gamma_1 = .2$.

(5) Smagorinsky's form of A with $\gamma_1 = .13$.

(6) Leith's form of A (Equation 5) with $\gamma_2 = .5$.

(7) Leith's form of A with $\gamma_2 = .2$.

In each experiment, the time-dependence of total kinetic energy, total enstrophy, and the total magnitude of the gradient of vorticity squared were calculated, along with the spectral distribution of energy and enstrophy. The effects of each dissipation form on these measurements and on typical wave disturbances were of prime interest.

Comparing first the time-dependence of kinetic energy (Figures 2, 3, 4), it was noted that except for the zero dissipation, zero source case there was a tremendous decrease of kinetic energy initially. The order in which this dissipation changed into regeneration was, by experiment numbers, 7,2,3,5,4,6. In general the Leith form halted the initial rapid dissipation of kinetic energy earlier.

The energy in the model at mid-time was, by decreasing order of magnitude, 1,5,7,2,4,3,6. These values were

obviously dependent upon the size of the dissipation term. However, the energy present at end-time was not in the same order as above, 1,5,7,4,3,2,6. This indicated the A = constant form had a greater rate of dissipation than the other forms after the source term was taken out. An interesting point noted was that for both A_L and A_S, the smaller γ terms produced the greater rate of dissipation. This was due to the dependence of both A_L and A_S on the strength of the flow and with the smaller γ the flow was stronger as will be discussed later.

Looking next at the time-dependence of enstrophy (Figures 5,6,7), in each of the experiments it was easily seen that enstrophy was far more conservative than energy. However, the enstrophy dissipated rapidly initially as did the kinetic energy. In the Smagorinsky and Leith forms of A there was a tendency for the enstrophy to stabilize faster for larger values of γ. Leith's form caused a slight growth in enstrophy after the initial drop but once the source was cut off at mid-time enstrophy dissipated slightly. In Smagorinsky's form, enstrophy was more nearly conserved while the source was in Equation (1), but enstrophy had a tendency to be dissipated when the source was turned off. A constant A did not conserve enstrophy.

The final time-dependent term to be considered was the total gradient of vorticity squared (Figures 8,9,10). This term was even more conservative than the two terms considered before. There was a tendency for equilibrium with respect

to $|\nabla\zeta|^2$ to be reached faster the greater the γ terms. The fastest equilibrium solution was from experiment 6 with experiment 3 following. The experiments in which the total gradient of vorticity squared was most conserved were both Leith forms and the Smagorinsky form with γ=.5, while there were a number of small fluctuations in 2. The deviations noted in the gradient of vorticity squared terms seemed to be more like step functions than smooth curves after the initial level-off of values in all experiments other than 1.

The next measurements to be considered were the spectral distributions of kinetic energy and enstrophy (Figures 11-18). The scalar energy spectrum and the scalar enstrophy spectrum were plotted on logarithmic scales at the initial time, 1512 time steps, and 3024 time steps. At the 1512th time step the source term was taken out of Equation (1). The 3024th time step was the final time step. The values of kinetic energy and enstrophy used in the spectral analysis were taken off the middle grid row, K=8. Since there were 25 grid points east-west, it was possible to obtain 12 wavenumbers. Components with wavenumbers greater than 6 are subject to possible distortion from aliasing errors.

In the initial spectra of kinetic energy and enstrophy, the energy and enstrophy were mainly contained in the even wavenumbers, which was due to the form of the initial stream field, and evenly distributed in these wavenumbers.

The zero dissipation, zero source experiment spectra had no discernible pattern other than a tendency for both energy

and enstrophy to be spread fairly evenly in all wavenumbers. Experiment 2, where A was a constant, concentrated energy and enstrophy in the lower even wavenumbers without any distinctive pattern.

In experiment numbers 3, 4, and 5, there was a tendency for a -3 power slope to become apparent in the plots of the spectral variation. It was noted in the A_S form, as γ became smaller the spectral distribution tended to "bend" away from the -3 power slope. The dropoff at the large wavenumbers end of the spectrum also became more pronounced as γ became smaller. Obviously, the amount of energy and enstrophy present in corresponding wavenumbers was increased with decreasing γ.

Experiment numbers 6 and 7 had a sawtooth appearance with the even numbered waves generally containing more energy than the odd numbered waves. The envelope of the spectral distribution did have a tendency toward the -3 power slope, with the strongest tendency appearing at mid-time. Enstrophy tended to approach the -3 power slope more nearly than kinetic energy.

For a comparison of the effects of the different dissipation forms on the wave disturbances, the stream function field was analyzed at the initial time and after time steps 756, 1512, 2268, 3024 or approximately every 5 days (Figures 19-47). All experiments were started with the same initial ψ field. The zero dissipation, zero source experiment may be referenced in the figures.

After time step 756, the stream function field was beginning to become quite zonal in character. It appeared to have

primarily long wave components that were dominated by wavenumber 2. The strongest flow pattern was in the experiments with the smallest γ and in the A = constant case. Low areas were situated in the zonal band around the middle grid row, K=8. High areas were along the north-south boundaries.

At time step 1512, mid-time for all experiments, the flow pattern was very zonal. The low areas again were along the middle grid rows thereby causing easterly flow in the north and westerly flow in the south. The experiments with the most zonal flow were 7, 5 and 2. Leith's form of dissipation with γ=.5 produced the least zonal flow with a wave form more obvious than the other forms of dissipation.

After time step 2268, the flow is still predominately zonal; however, it had become weaker and was starting to deform in all experiments, the most notable cellular circulation being in A_L with γ=.5.

At the end-time of the experiments, the flow had considerably weakened. Leith's form of dissipation, with γ=.2 and the A=constant form stream function patterns were still very zonal in nature. Smagorinsky's forms deviated from the zonal flow more as the γ term decreased. The Smagorinsky form with γ_1=.13 had cellular circulation corresponding to about wavenumber 2. Leith's form with γ=.5 had the weakest flow pattern and the least zonal.

V. CONCLUSIONS

Leith's form of dissipation was the fastest acting of the dissipation forms. All of the time-dependent curves reached their minimum value faster with A_L. After the dissipative effect had leveled off the source term had become dominant and the A_L forms had more of an opportunity to grow, with the smallest γ coefficients growing most rapidly. The spectral curves showed that A_L had a tendency to form an envelope which approximately fit the -3 power slope. The variation in the constant γ in Leith's form of dissipation had the greatest influence on the stream field.

Smagorinsky's form for dissipation was not as fast acting as Leith's form. The Smagorinsky's form was also not as sensitive to the constant coefficient as was A_L, i.e., all measurements made with different γ's indicated well behaved curves that related almost one to one with each other. For the A_S form, the spectral distributions between wavenumbers 1 to 6 fit the -3 power slope fairly well, with γ_1=.2 being the best fit. The stream function field for A_S was generally the least zonal of the forms of dissipation considered, with the strength of the flow inversely dependent upon the constant coefficients. The more zonal the flow, the stronger the gradients of the stream function appeared.

The constant form of A had the slowest reaction time in the time-dependence measurements as long as the source term was still in Equation (1). However, A_C produced the greatest

variations when the source term was removed in the time-dependence measurements. In the spectral measurements, the A_C form tended to have the -3 power slope in the even numbered waves only. The stream function field produced by A_C moved toward zonal flow at about the same rates as the other forms; however, once the zonal flow was established, A_C form kept the zonal flow more than the other forms.

Due to the simplicity of the model used in this study and the use of synthetic initial data, it is impossible to conclude which form of dissipation is the best in meteorological terms. However, this author believes that the differences in the experiments performed are great enough to justify further studies of this nature.

Additional experiments that appear desirable are the following:

First the expanding of the grid to investigate more wavenumbers.

Secondly, the addition of a linear drag term on the right hand side, namely, $-K\zeta$, to simulate the surface friction forces at work in the atmosphere.

Thirdly, and probably the most important, changing the source term to better simulate the baroclinic processes of the real atmosphere, with the source term having an effective wavenumber between 7 and 8.

It is expected that these variations to this model would produce a more realistic spectral distribution, and in accordance with two-dimensional turbulence theory. Hopefully,

the new formulation would produce a stream function field that was meteorologically meaningful.

APPENDIX A

COMPLETE DESCRIPTION OF THE MODEL

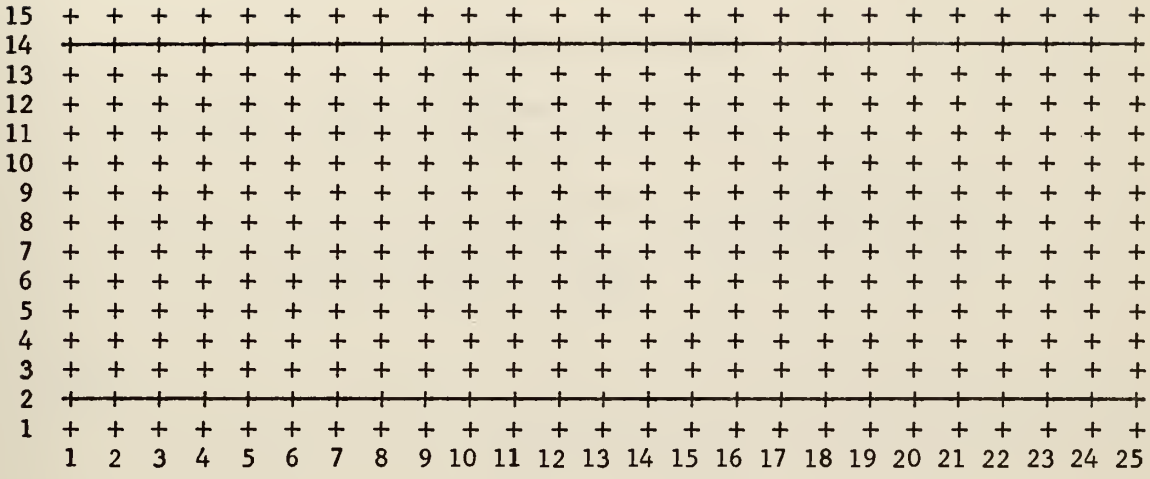

Figure 1. Grid for the model.

North-south direction has 15 grid points indexed with K. East-west direction has 25 grid points indexed with J. Distance between grid points was 2.5^{o} latitude or 150 nautical miles ($\Delta x=\Delta y=2.5^{o}$). The grid is imposed on a constant β plane located at 45^{o}N (K=8).

BOUNDARY CONDITIONS

The southern boundary was placed at K=2 and the northern at K=14. The stream function was set equal to zero along these boundaries, i.e.

$$\psi(J,2) = \psi(J,14) = 0$$

To insure free slip on the northern and southern boundaries

$$\psi(J,1) = - \psi(J,3)$$

and

$$\psi(J,15) = - \psi(J,13)$$

was imposed on the model.

Periodicity was assumed in the east-west direction and achieved by:

$$\psi(1,K) = \psi(26,K)$$

and

$$\psi(25,K) = \psi(0,K)$$

INITIAL CONDITIONS

The initial stream function was defined as:

$$\psi(J,K) = - C \sin\left(\frac{4\pi x}{L}\right) \sin\left(\frac{\pi y}{W}\right) - C \sin\left(\frac{8\pi x}{L}\right) \sin\left(\frac{\pi y}{W}\right) - C \sin\left(\frac{12\pi x}{L}\right) \sin\left(\frac{\pi y}{W}\right)$$

where

$X = (J-1)\ \Delta x$ $\qquad$ $J = 1,2,\ldots,25$

$Y = (K-3)\ \Delta y$ $\qquad$ $K = 3,4,\ldots,16$

$W = 12\ \Delta y$ $\qquad$ (width between north-south boundaries)

$L = 2W\ \Delta x$ $\qquad$ (length of grid periodicity)

$C = 1.0 \times 10^{7}$

The source term was related to the stream function by

$$S = - S_o\ \psi/C$$

where $S_o = 1.0 \times 10^{-10}$.

APPENDIX B

FINITE DIFFERENCE EQUATIONS

Equations (1), (2), and (3) are solved numerically by introducing finite-differences in x, y, and t. Sequential over-relaxation was used to solve for the ψ field and is discussed in Appendix C. Time differencing is discussed in Appendix D.

The vorticity, or the Laplacian of ψ, was approximated by the second-order expression using the center and four immediately contiguous points.

$$\zeta = \nabla^2\psi = [\psi(J+1,K)+ \psi(J-1,K)+ \psi(J,K+1)+ \psi(J,K-1)-4\psi(J,K)]/(\Delta x)^2 \equiv \nabla\psi(\Delta x)^2$$

The numerical space-differencing method used on the non-linear term on the left hand side of Equation (1) is the second-order scheme developed by Arakawa (1966), which conserves kinetic energy and enstrophy within the nonlinear term.

$$J(\psi,\zeta) = - J(\zeta,\psi)$$

$$\begin{aligned} J(\zeta,\psi) = \frac{1}{3}\Big(&\Big\{[\zeta(J+1,K) - \zeta(J-1,K)]\,[\psi(J,K+1) - \psi(J,K-1)] \\ &-[\zeta(J,K+1) - \zeta(J,K-1)]\,[\psi(J+1,K) - \psi(J-1,K)]\Big\}\ /4(\Delta x)^2 \\ &+\Big\{\zeta(J+1,K+1)[\psi(J,K+1)-\psi(J+1,K)]- \zeta(J-1,K-1)[\psi(J-1,K)- \psi(J,K-1)] \\ &+\ \zeta(J+1,K-1)[\psi(J+1,K)-\psi(J,K-1)]- \zeta(J-1,K+1)[\psi(J,K+1)- \psi(J-1,K)]\Big\} \\ &/4(\Delta x)^2 \\ &+\Big\{\zeta(J+1,K)[\psi(J+1,K+1)-\psi(J+1,K-1)]- \zeta(J-1,K)[\psi(J-1,K+1)-\psi(J-1,K-1)] \\ &- \zeta(J,K+1)[\psi(J+1,K+1)-\psi(J-1,K+1)]+ \zeta(J,K-1)[\psi(J+1,K-1)-\psi(J-1,K-1)]\Big\} \\ &/4(\Delta x)^2\Big) \end{aligned}$$

The linear β term in Equation (1) was approximated by the first order difference equation

$$\beta\,\frac{\partial\psi}{\partial x} = \beta\left\{[\psi(J+1,K) - \psi(J-1,K)]/2\Delta x\right\}$$

The above procedure was also used to find the finite difference form of the wind velocity components.

For the final term in Equation (1), an imaginary staggered grid had to be imposed. This half grid was needed because the finite differencing procedure limited the values obtainable. The form of the viscosity term was

$$\begin{aligned}\nabla \cdot (A\nabla\zeta) = &\Big(\Big\{[\zeta(J+1,K)- \zeta(J,K)]/\Delta x\Big\} \quad \Big\{[A(J+1,K) + A(J,K)]/2\Big\} \\ &- \Big\{[\zeta(J,K)- \zeta(J-1,K)]/\Delta x\Big\} \quad \Big\{[A(J,K) + A(J+1,K)]/2\Big\}\Big) \\ &+ \Big(\Big\{[\zeta(J,K+1)- \zeta(J,K)]/\Delta y\Big\} \quad \Big\{[A(J,K+1)+ A(J,K)]/2\Big\} \\ &- \Big\{[\zeta(J,K)- \zeta(J,K-1)]/\Delta y\Big\} \quad \Big\{[A(J,K) + A(J,K+1)]/2\Big\}\Big)\end{aligned}$$

APPENDIX C

RELAXATION TECHNIQUE

The equation to be solved for the $\partial\psi/\partial t$ field from Equations (1) and (3) is

$$\nabla^2 \frac{\partial \psi}{\partial t} = F(x,y) \tag{C-1}$$

where

$$F(x,y) = J(\zeta,\psi) - \beta \frac{\partial \psi}{\partial x} + S + \nabla \cdot (A\nabla\zeta) \ , \tag{C-2}$$

subject to the boundary conditions, $\partial\psi/\partial t = 0$ on the north-south boundaries and periodic in the east-west direction.

In the numerical experiments, F(J,K) was computable on all interior grid points and the boundary conditions were known. Therefore, values of $\partial\psi/\partial t(J,K)$ were determinable from the Poisson equation

$$\nabla^2 \frac{\partial \psi}{\partial t}(J,K) = F_1(J,K) \tag{C-3}$$

where

$$F_1(J,K) = \text{finite difference form of } F(J,K)(\Delta x)^2 \tag{C-4}$$

The first step in the iterative technique of sequential over-relaxation for the solution of Equation (C-3) was to make a first guess of values of $\partial\psi/\partial t$ for every grid point to satisfy Equation (C-3). In these experiments this first guess after one step was zero everywhere; in subsequent steps the value from the previous time step was used for the guess field.

For every estimate of the solution, the residual is defined as follows:

$$R^N(J,K) \equiv \nabla^2 \frac{\partial \psi}{\partial t}^{(N)}(J,K) - F_1(J,K)$$

where the superscript denotes the iteration.

A new estimate was made according to the formula:

$$\frac{\partial \psi}{\partial t}^{(N+1)}(J,K) = \frac{\partial \psi}{\partial t}^{(N)}(J,K) + \frac{(1+\alpha)}{4} R^N (\Delta x)^2$$

where α is the overrelaxation coefficient and for these experiments equaled .65.

The iterations were continued until $|R^N(J,K)| \leq \epsilon$ for all J,K, where ϵ was taken to be 1.0×10^{-13} m^2 sec^{-1} at which time the solution was considered to be sufficiently accurate.

APPENDIX D

TIME STEP SCHEMES

In general, centered time differences (leapfrog) were used for all quantities; however, the first step was a Euler-backward time step. The latter was also introduced every 50 time steps to selectively damp high frequency waves and to prevent the separation of solutions at even and odd time steps caused by the leapfrog time scheme.

LEAPFROG SCHEME

$$\psi^{(t+1)}(J,K) = \psi^{(t-1)}(J,K) + 2\Delta t \frac{\partial \psi}{\partial t}^{(t)}(J,K)$$

where superscripts denote the time level.

EULER-BACKWARD

The Euler-backward is composed of two steps:

1. (forward step) $\psi^{(t+1)*}(J,K) = \psi^{(t)}(J,K) + \Delta t \frac{\partial \psi}{\partial t}^{(t)}(J,K)$
2. (simulated backward) $\psi^{(t+1)}(J,K) = \psi^{(t)}(J,K) + \Delta t \frac{\partial \psi}{\partial t}^{(t+1)*}(J,K)$

Time steps were 10 minutes and a total of 3024 steps (about 3 weeks) were taken in each experiment.

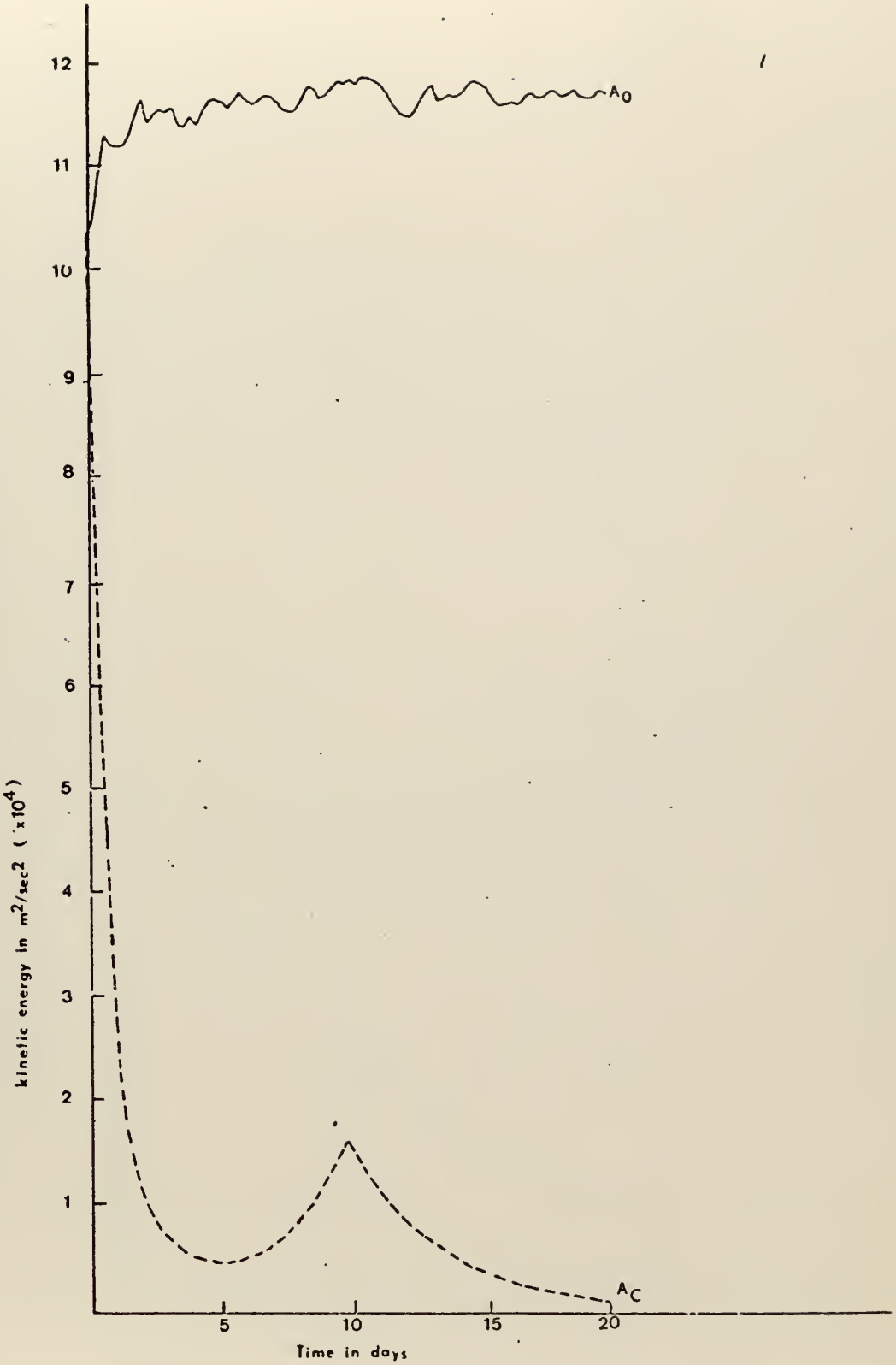

Figure 2. Total kinetic energy vs. time for the zero forcing and zero dissipation case and for A=constant form of dissipation

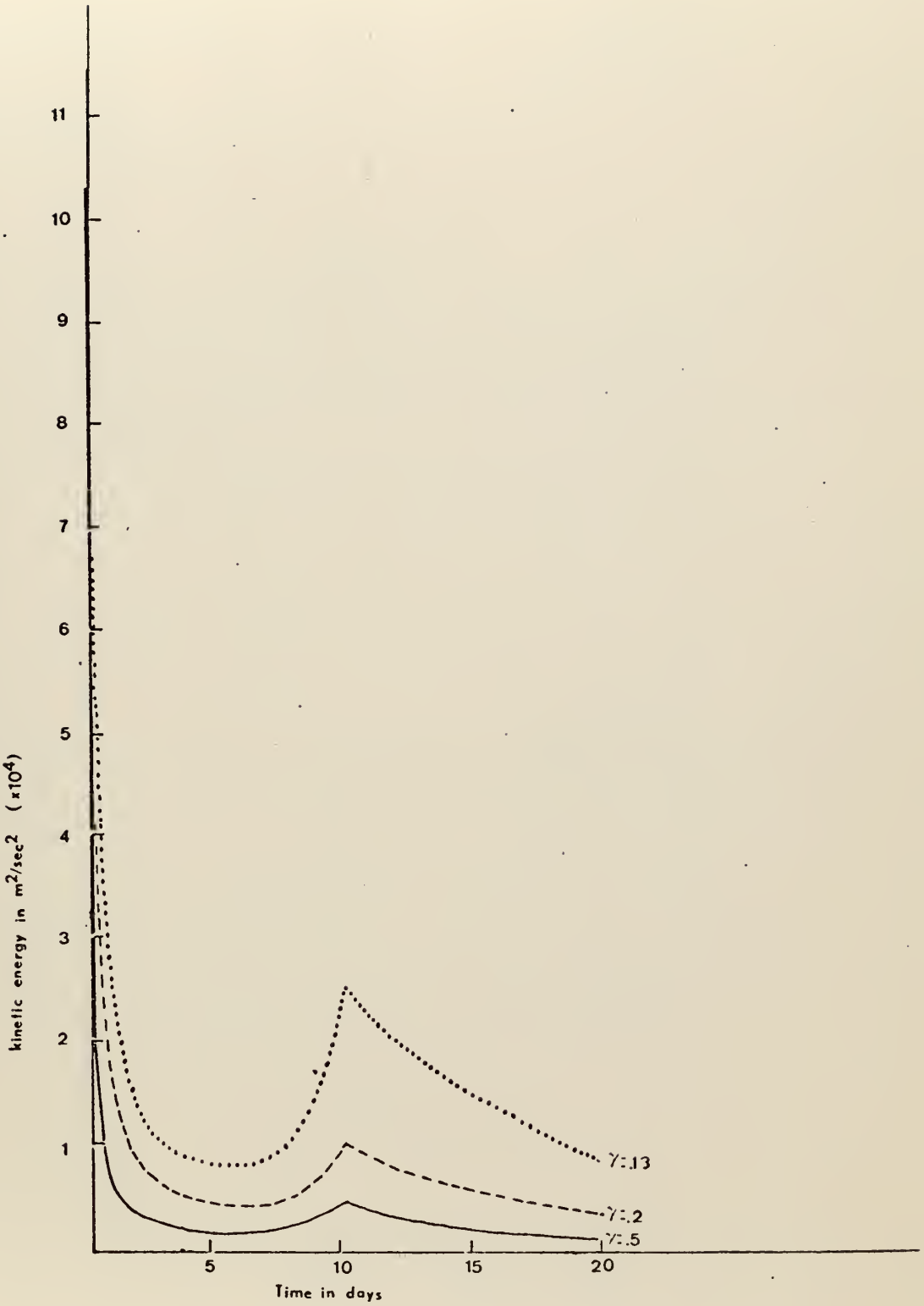

Figure 3. Total kinetic energy vs. time for the A_s form of dissipation with gamma=.5, .2, and .13

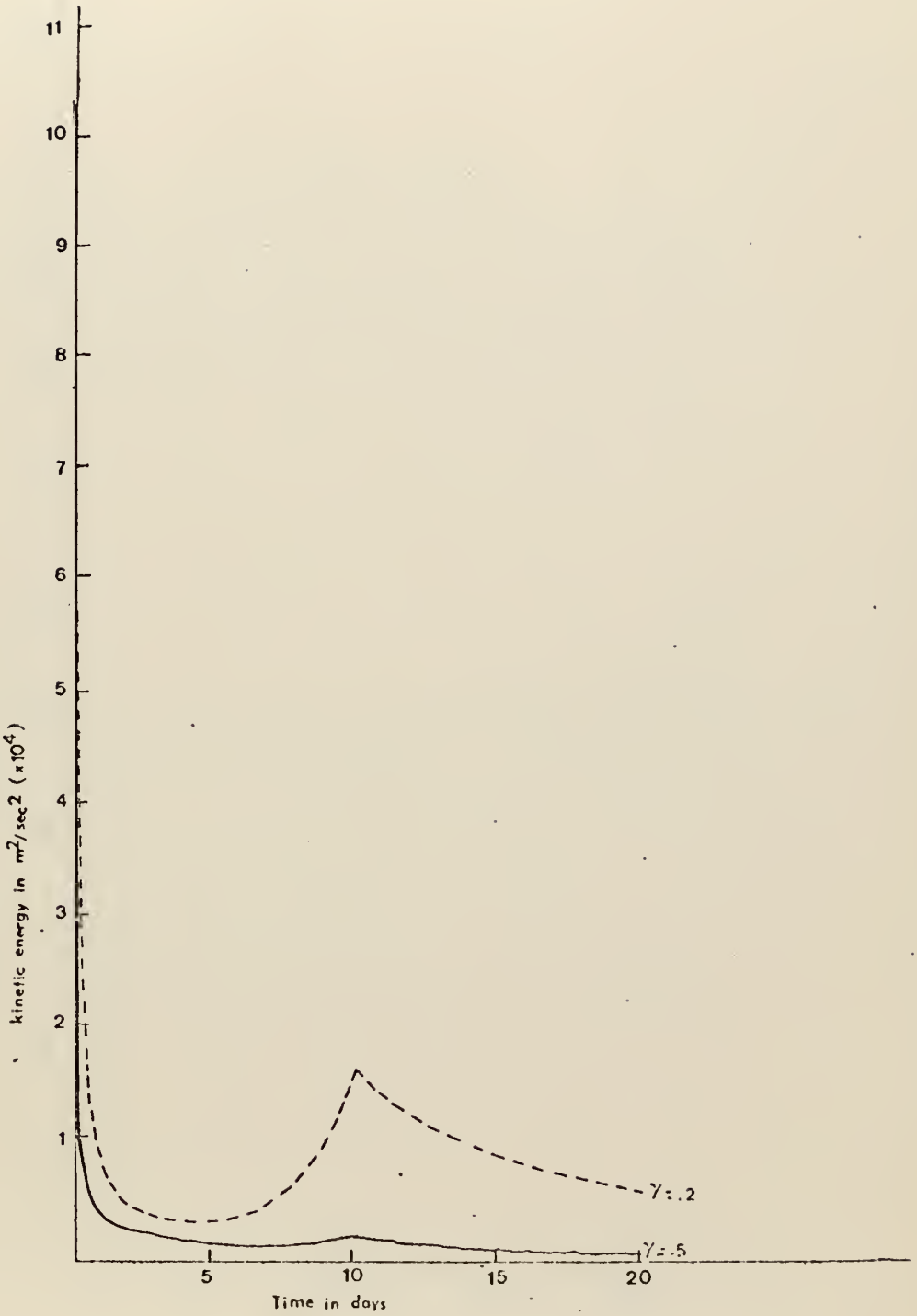

Figure 4. Total kinetic energy vs. time for the A_I form of dissipation with gamma=.5 and .2.

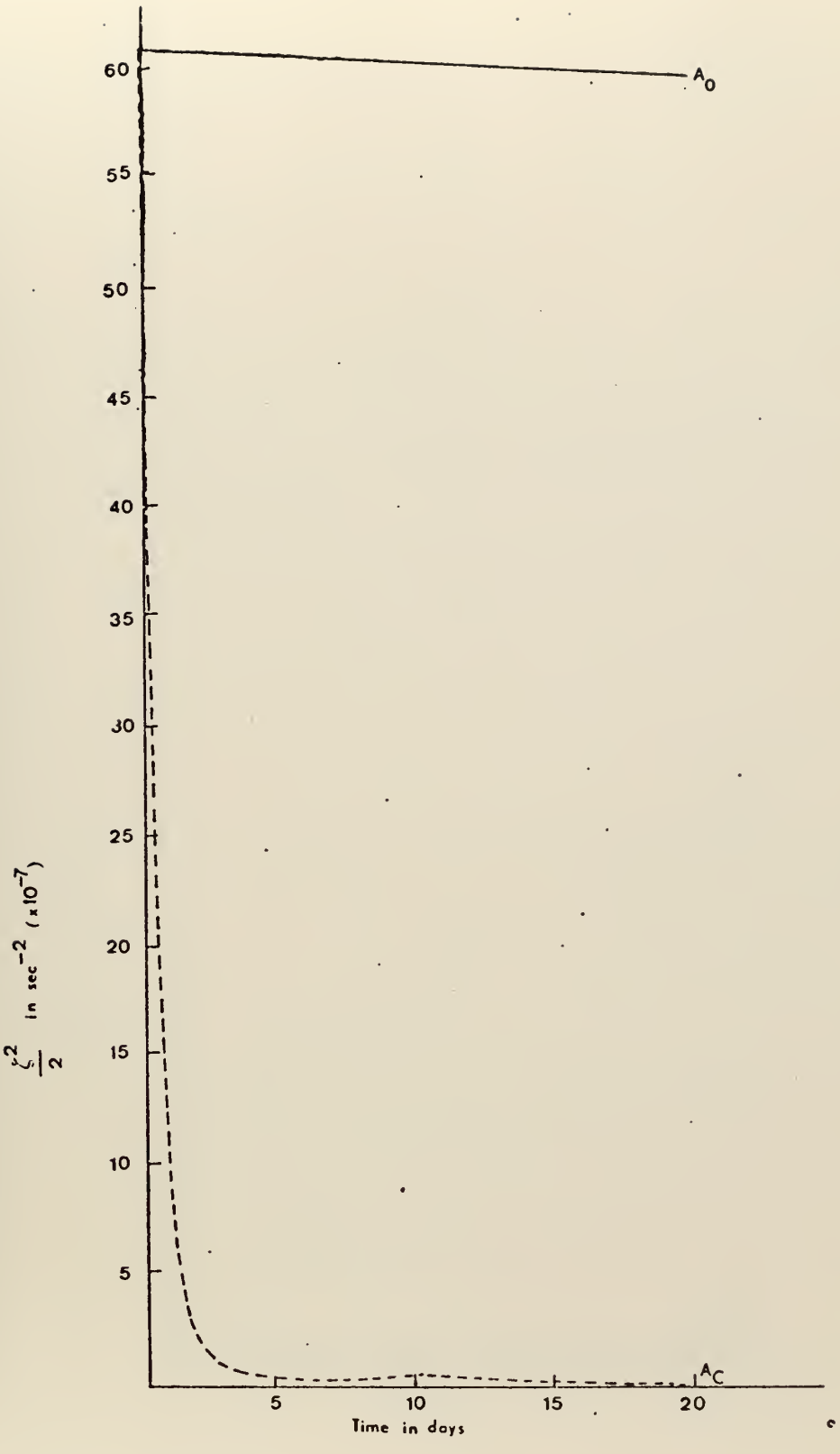

Figure 5. Total enstrophy vs. time for the zero forcing and zero dissipation case and for A=constant form of dissipation

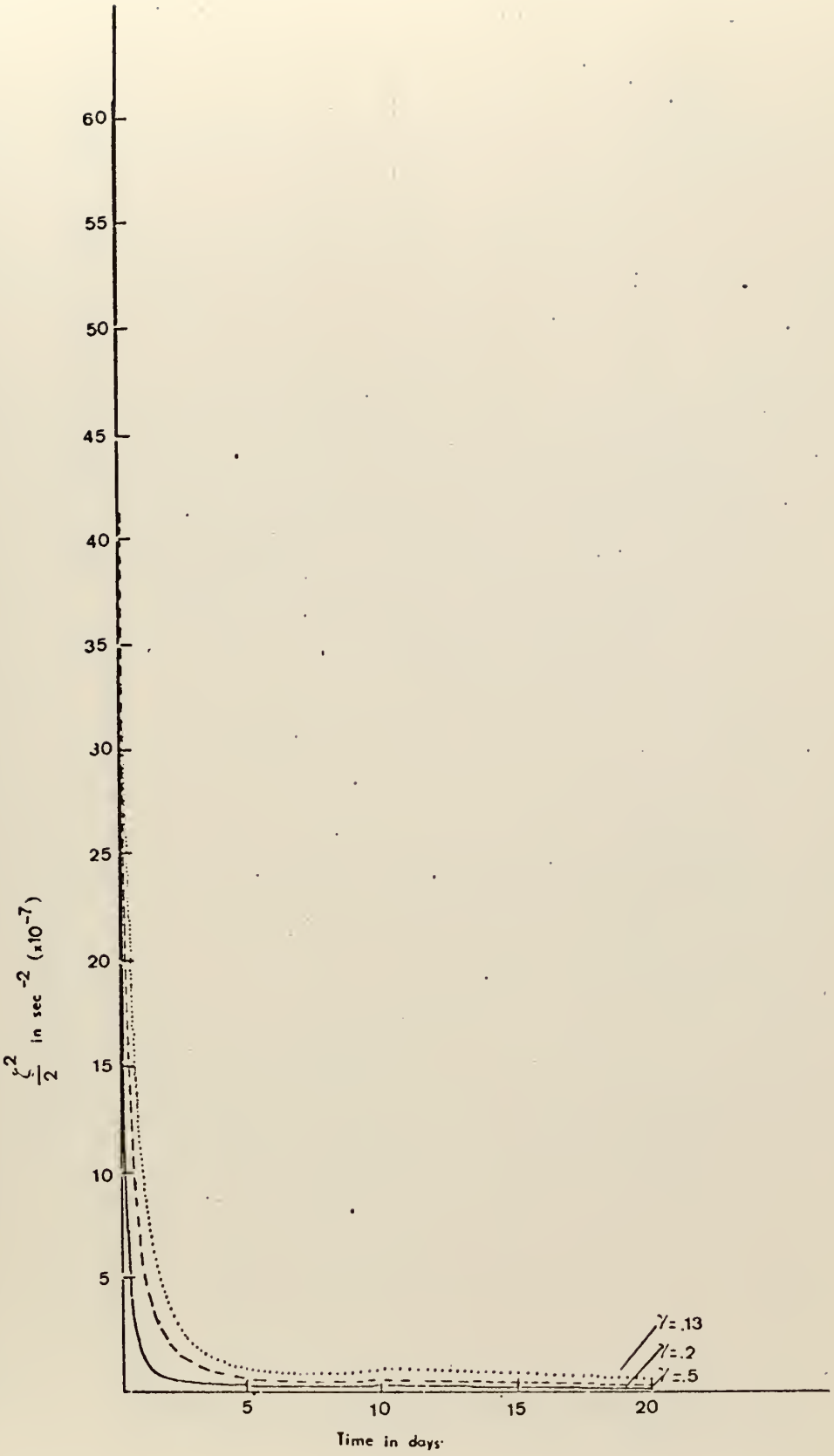

Figure 6. Total enstrophy vs. time for the A_s form of dissipation with gamma=.5, .2, and .13

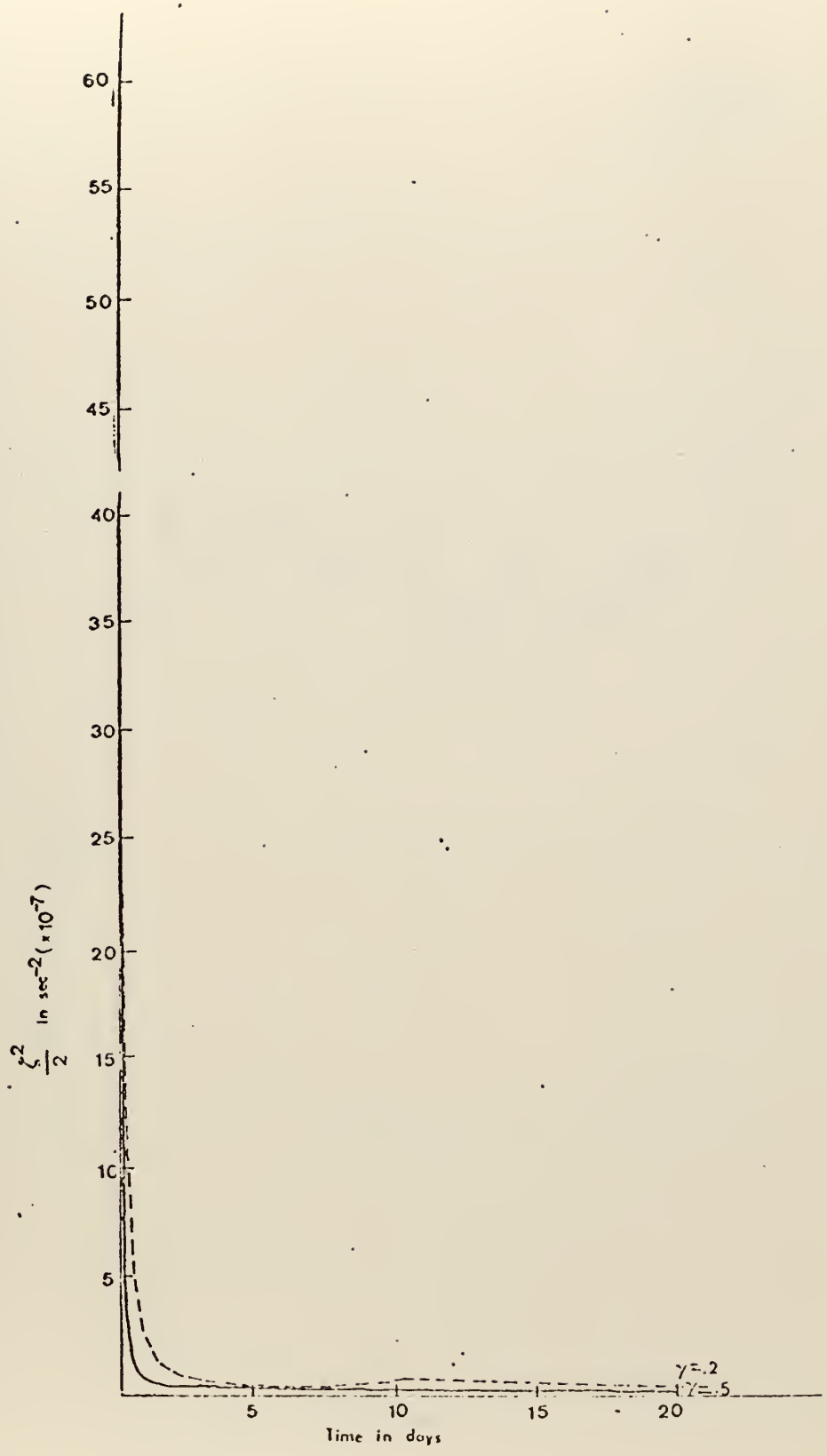

Figure 7. Total enstrophy vs. time for the A_L form of dissipation with gamma=.5 and .2

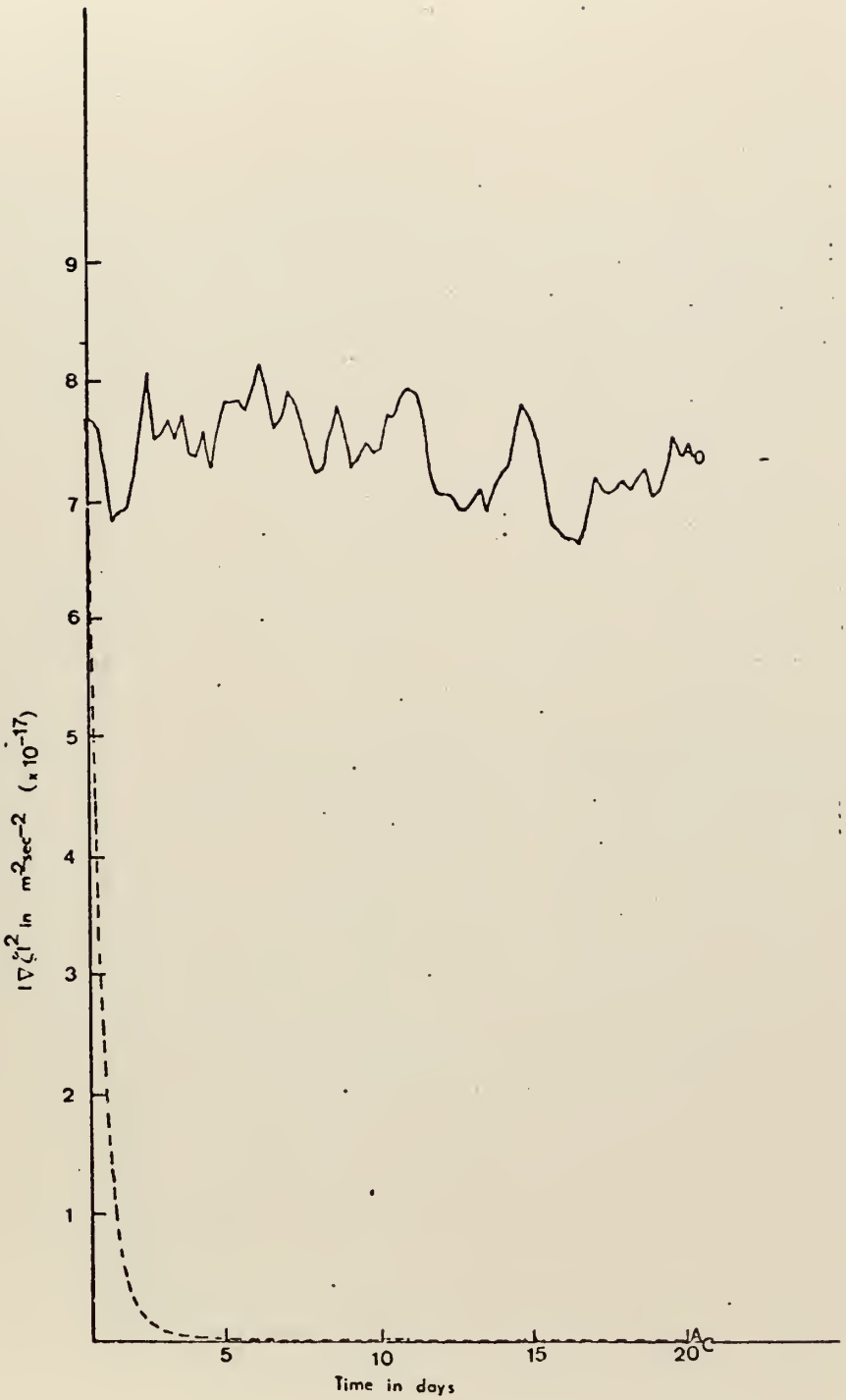

Figure 8. Total gradient of vorticity squared vs. time for the zero forcing and zero dissipation case and for A=constant form of dissipation

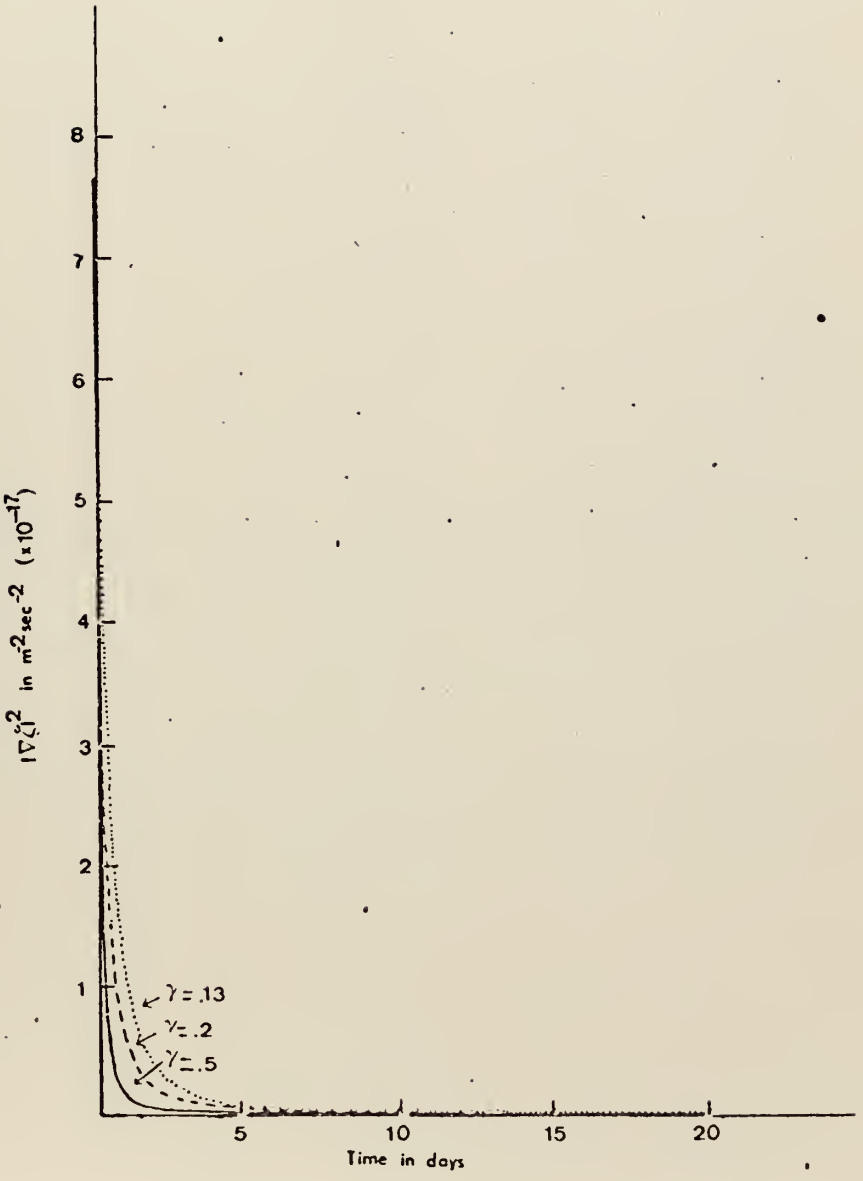

Figure 9. Total gradient of vorticity squared vs. time for the A_s form of dissipation with gamma=.5, .2, and .13

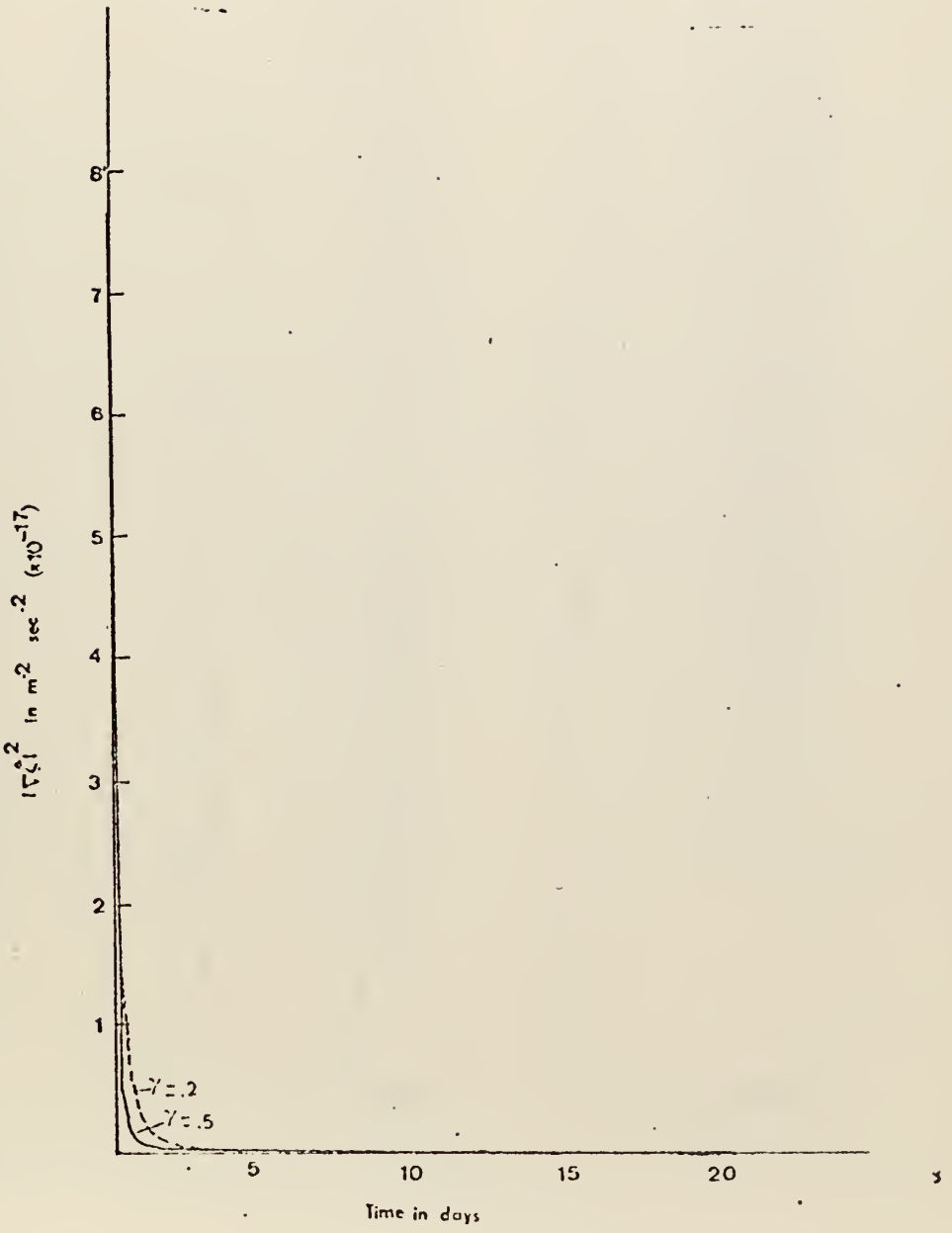

Figure 10. Total gradient of vorticity squared vs. time for the A_1 form of dissipatio with gamma=.5 and .2

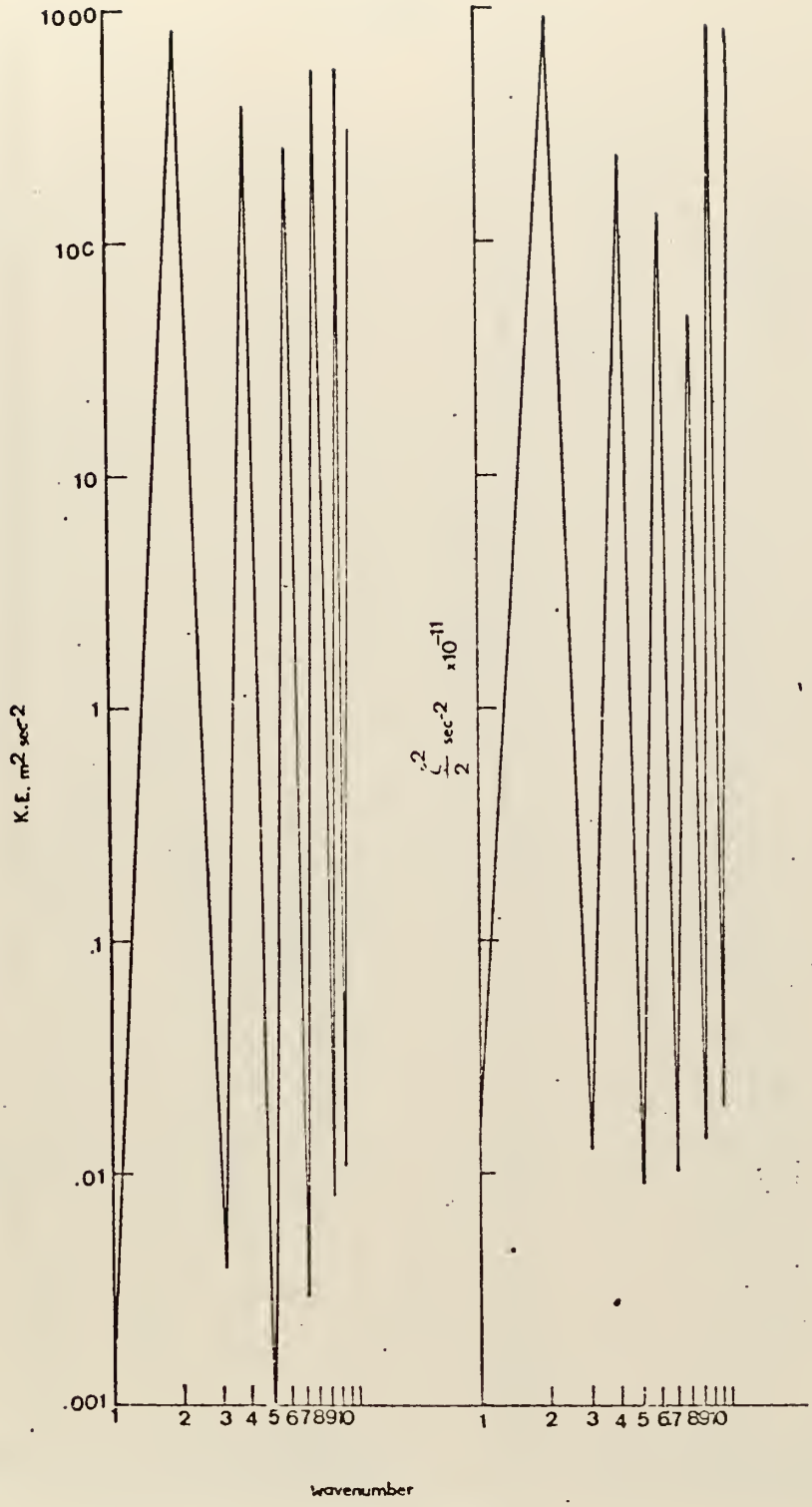

Figure 11. Initial spectral distribution of kinetic energy and enstrophy

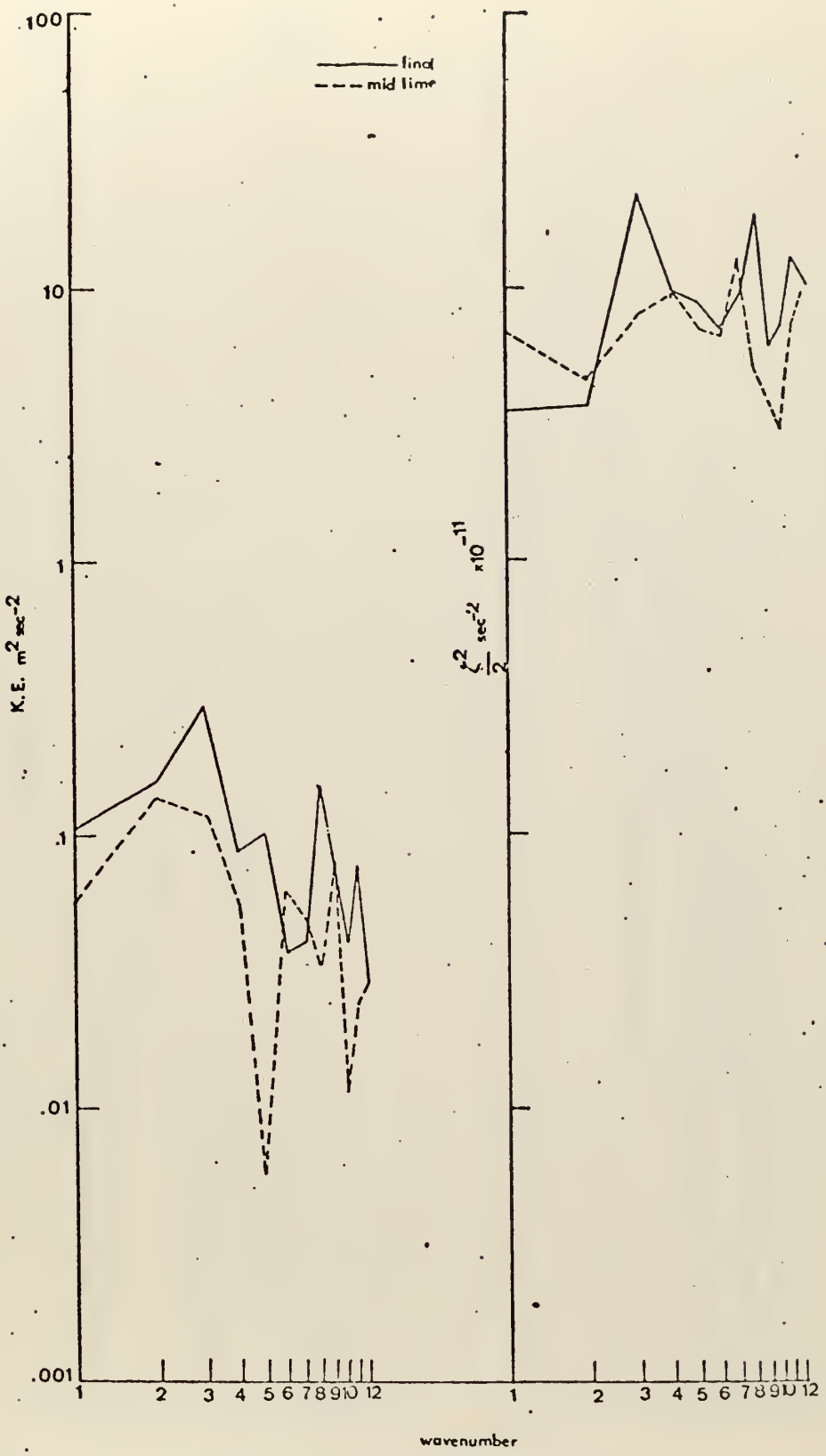

Figure 12. Spectral distribution of kinetic energy and enstrophy at mid-time and end-time for the zero dissipation and zero forcing case

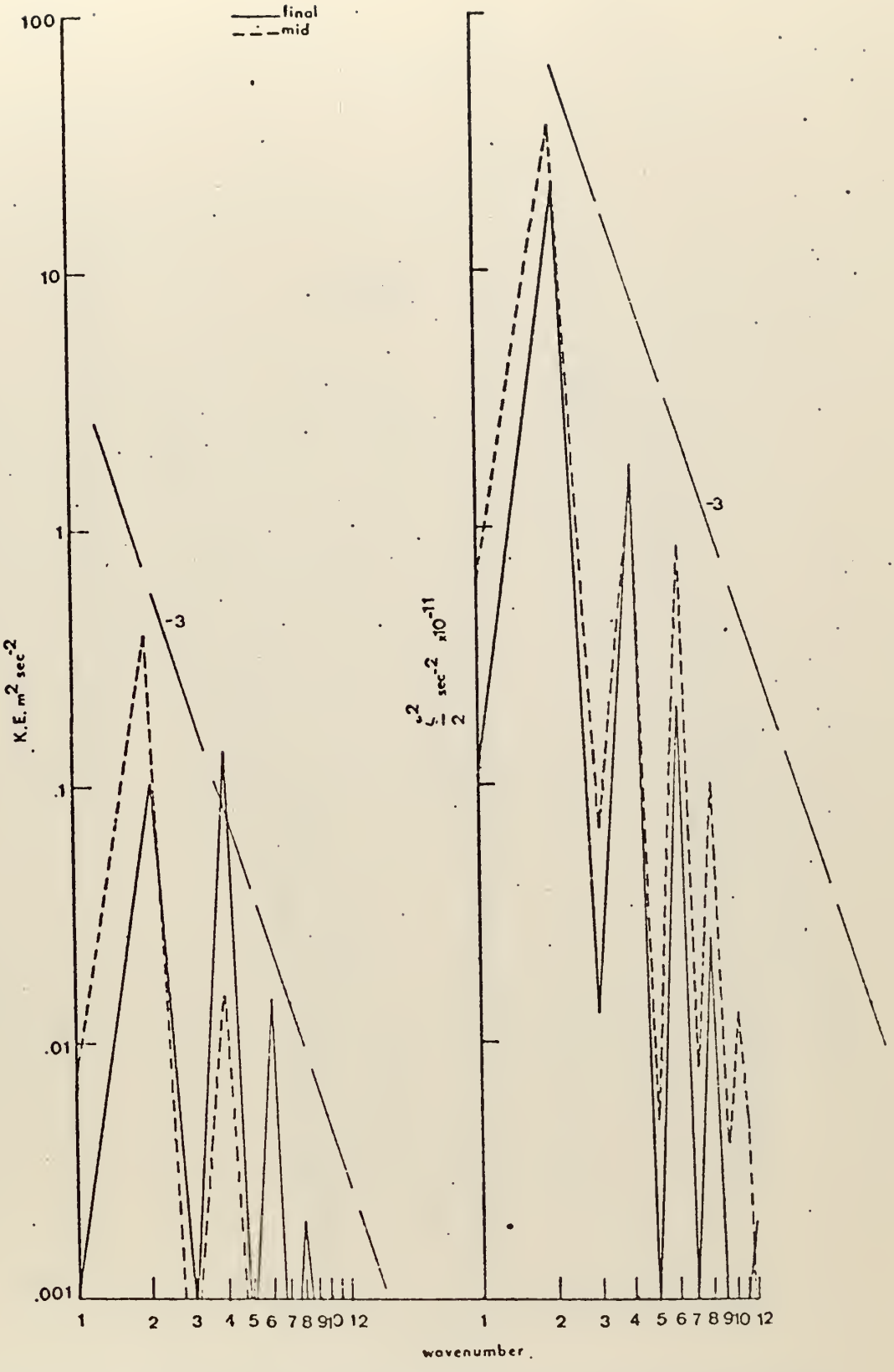

Figure 13. Spectral distribution of kinetic energy and enstrophy at mid-time and end-time for the A=constant form of dissipation

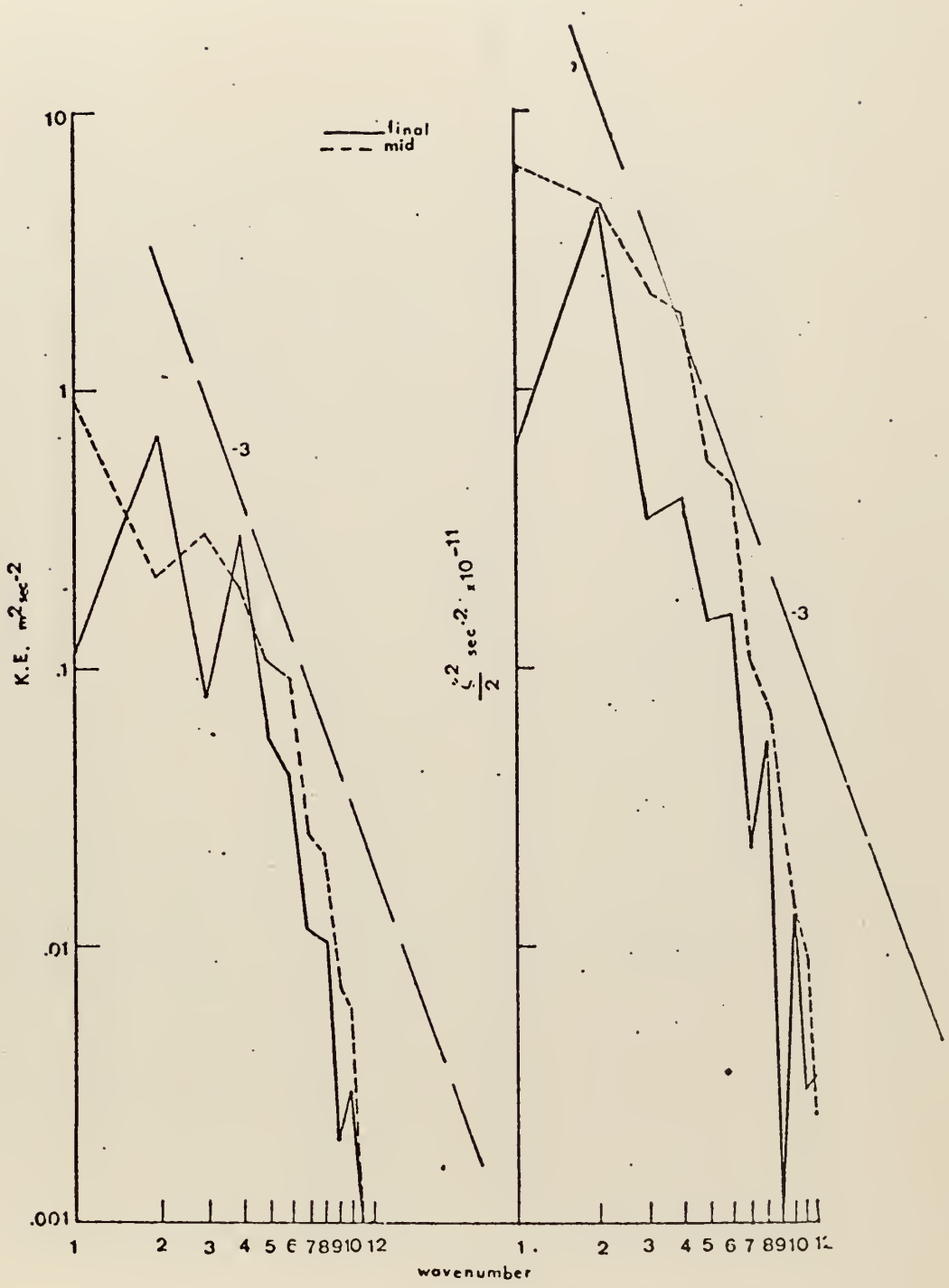

Figure 14. Spectral distribution of kinetic energy and enstrophy at mid-time and end-time for the A_S form of dissipation with gamma= .5

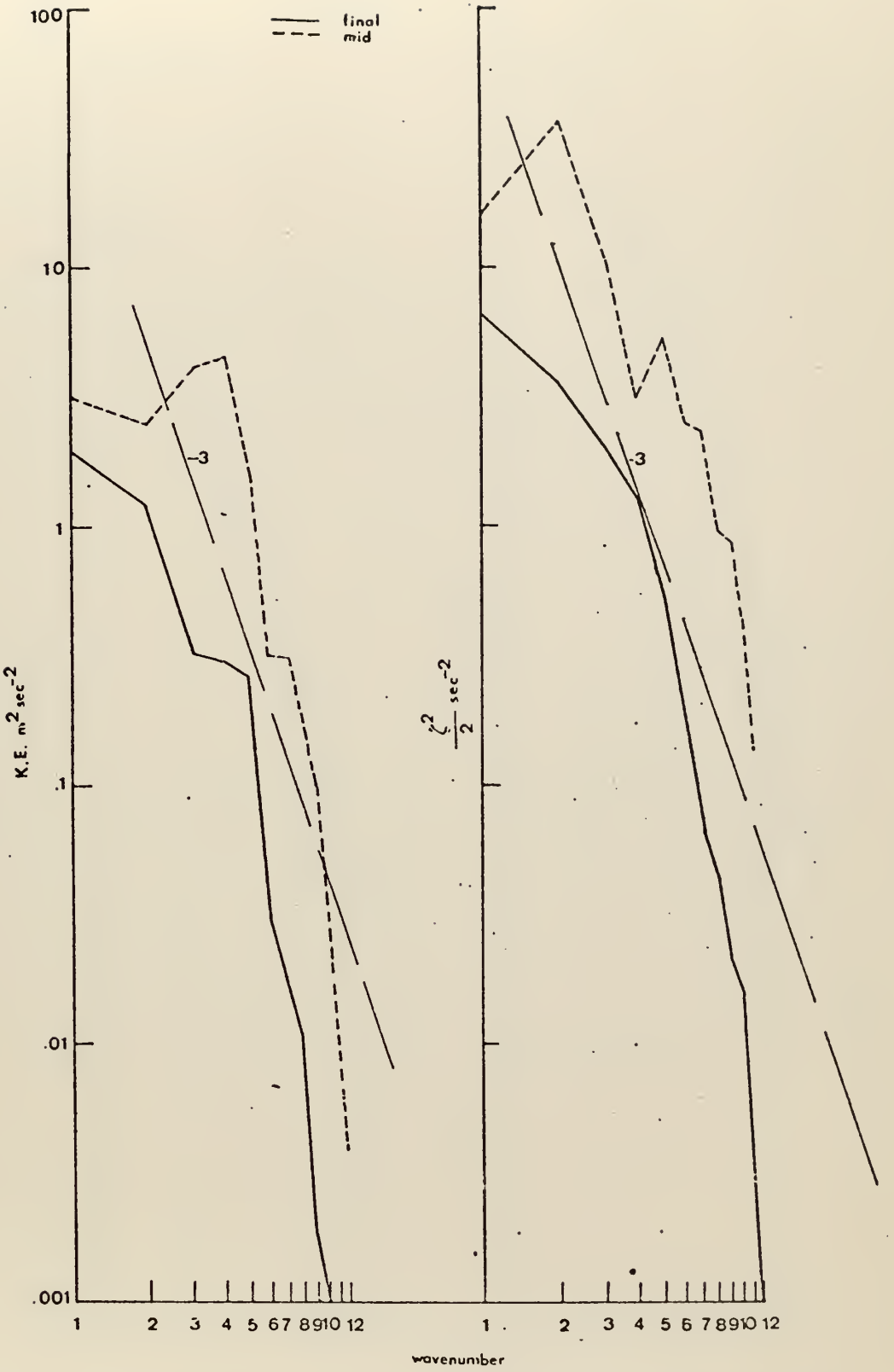

Figure 15. Spectral distribution of kinetic energy and enstrophy at mid-time and end-time for the A_s form of dissipation with gamma= .2

Figure 16. Spectral distribution of kinetic energy and enstrophy at mid-time and end-time for the A_s form of dissipation with gamma= .13

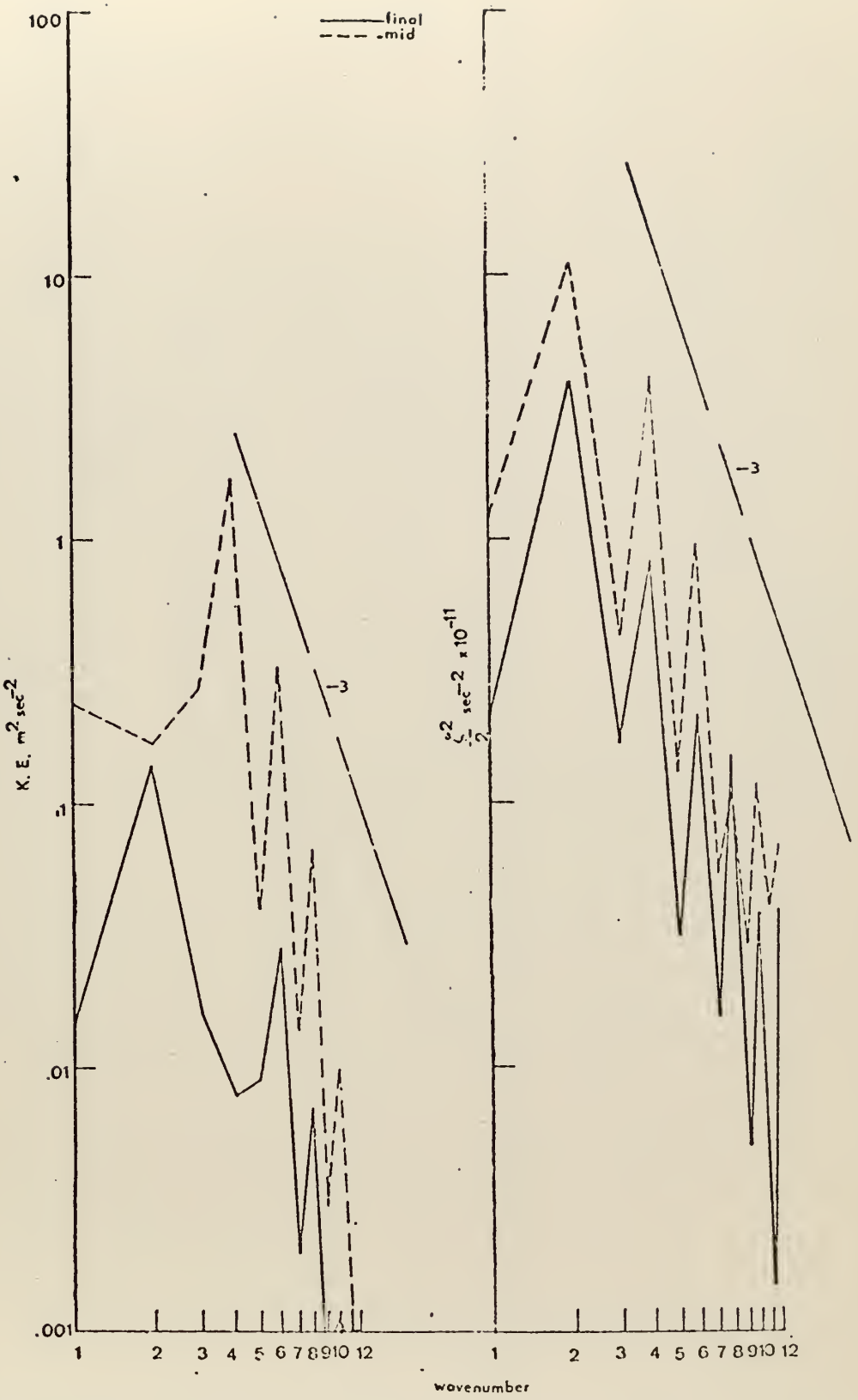

Figure 17. Spectral distribution of kinetic energy and enstrophy at mid-time and end-time for the A_L form of dissipation with g... .5

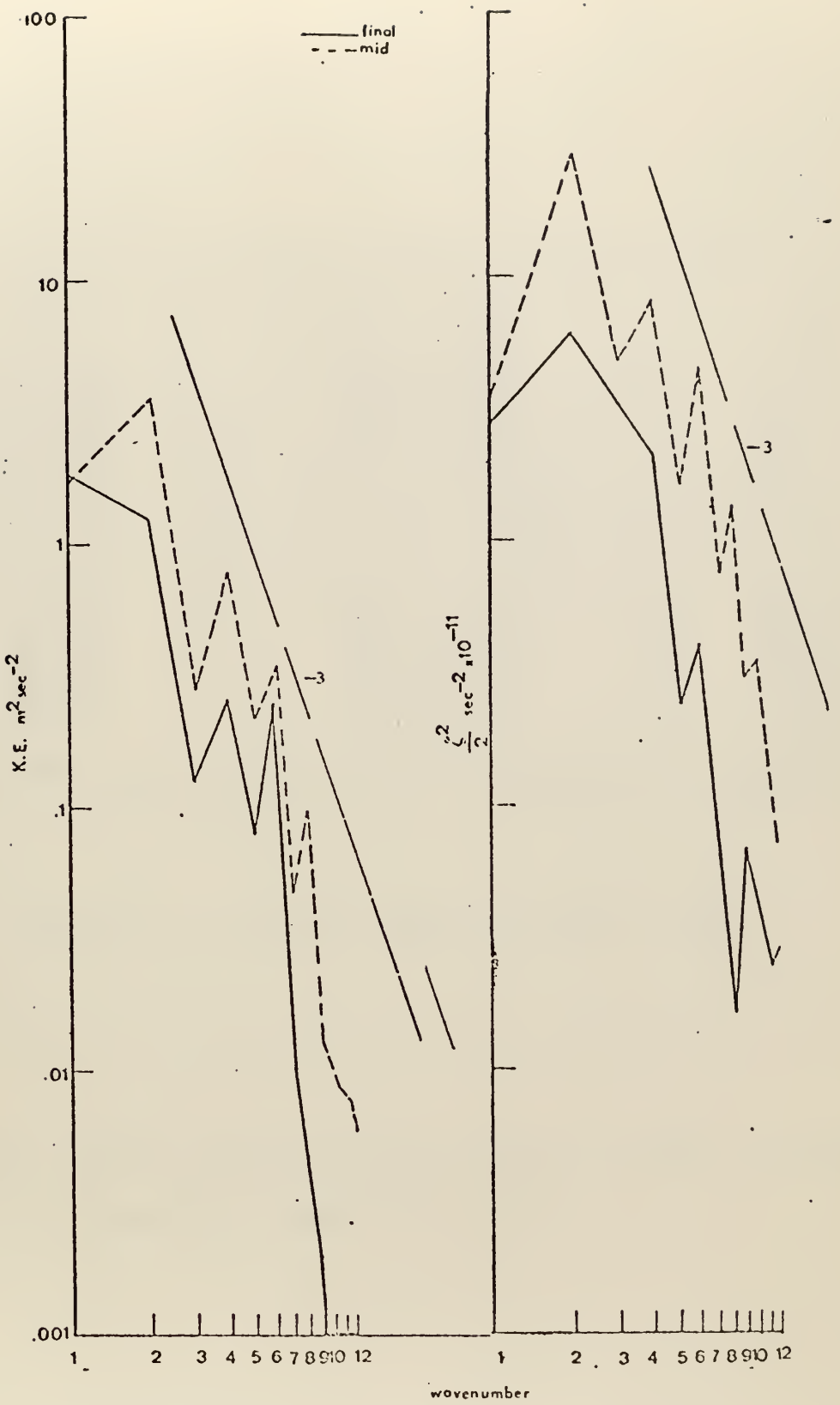

Figure 18. Spectral distribution of kinetic energy and enstrophy at mid-time and end-time for the A_L form of dissipation with γ = .2

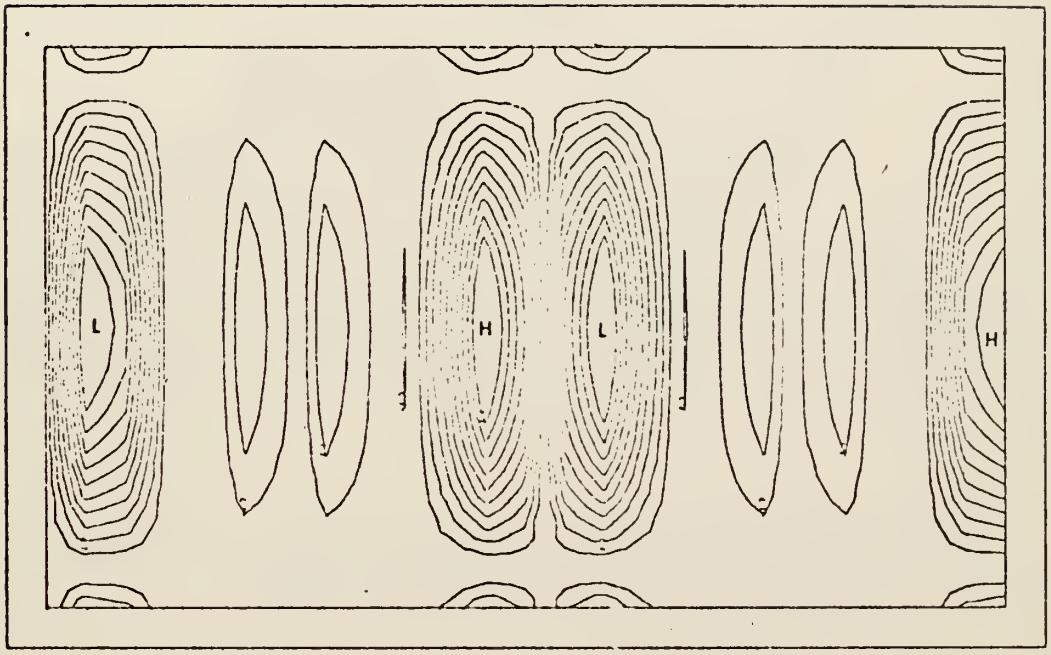

Figure 19. Initial stream function field

(All stream fields contoured from -2.0×10^7 to $+2.0 \times 10^7$ in increments of $.2 \times 10^7$ m^2 sec^{-1})

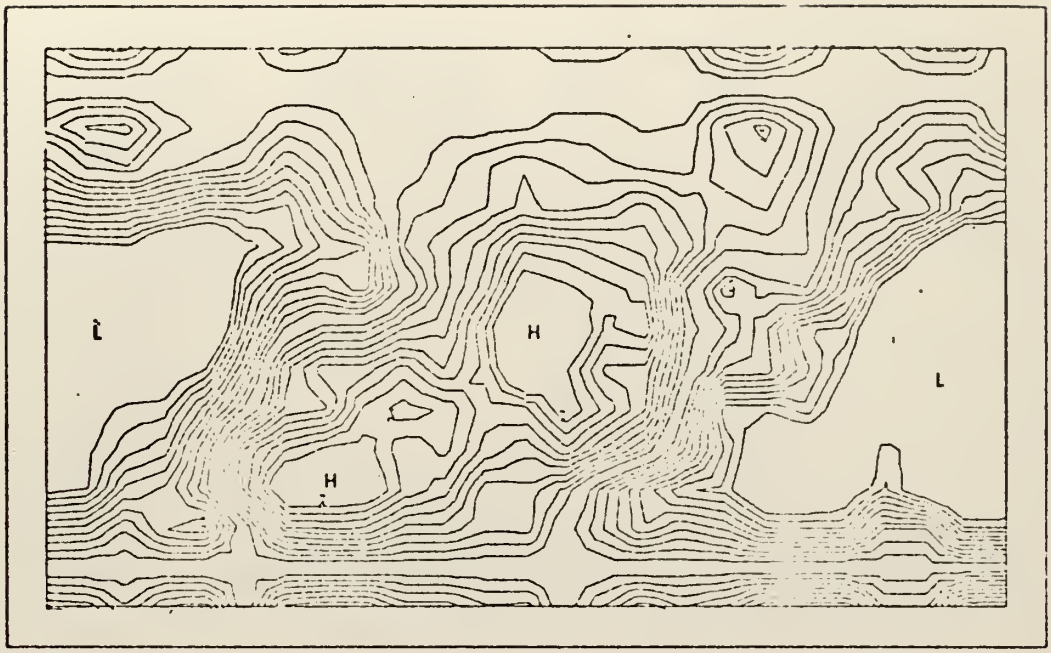

Figure 20. Stream function field at 5 days for zero forcing and zero dissipation case

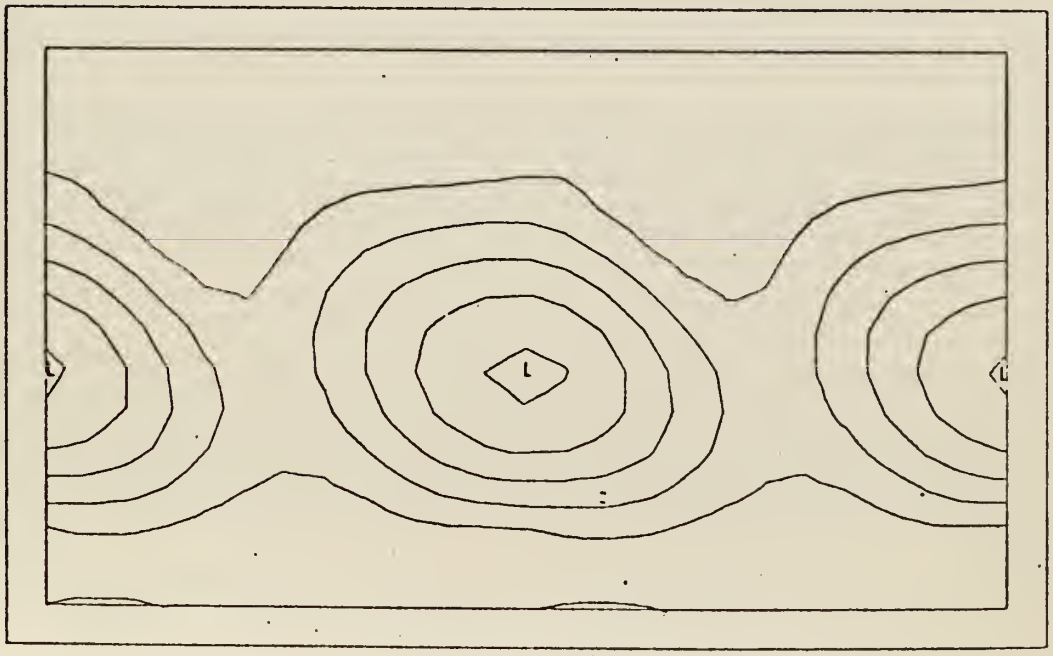

Figure 21. Stream function field at 5 days for A=constant form of dissipation

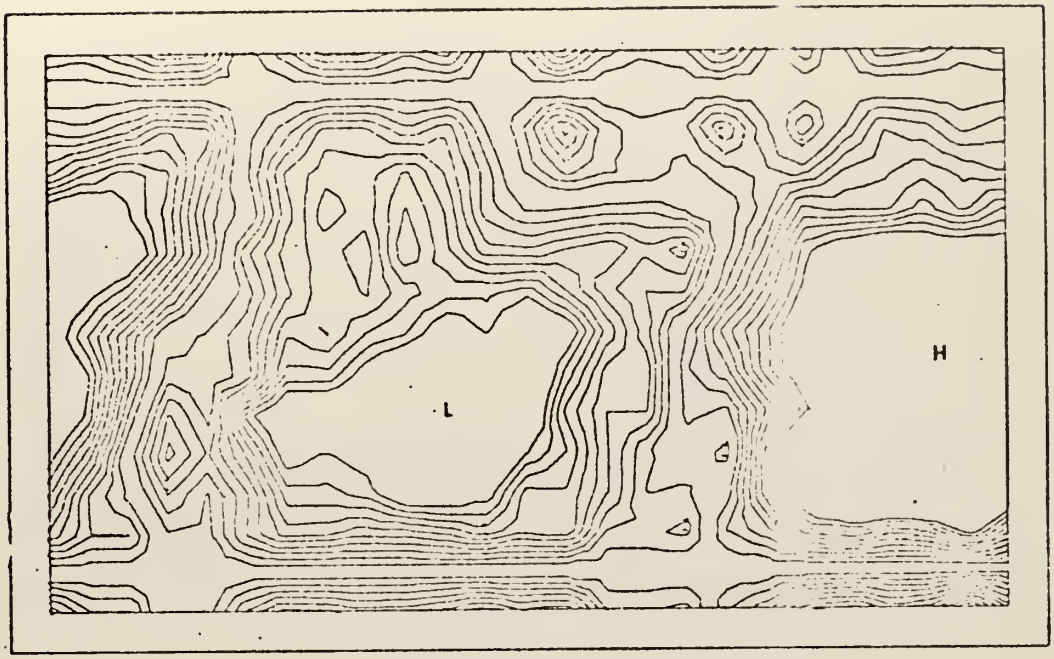

Figure 22. Stream function field at 10 days for zero forcing and zero dissipation case

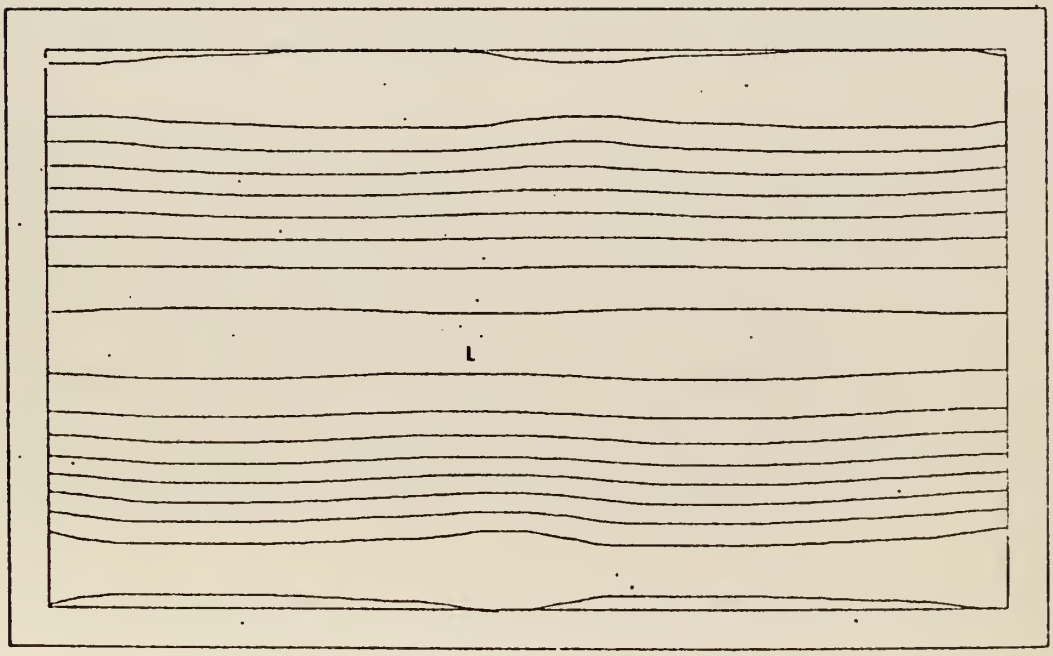

Figure 23. Stream function field at 10 days for A=constant form of dissipation

Figure 24. Stream function field at 15 days for zero forcing and zero dissipation case

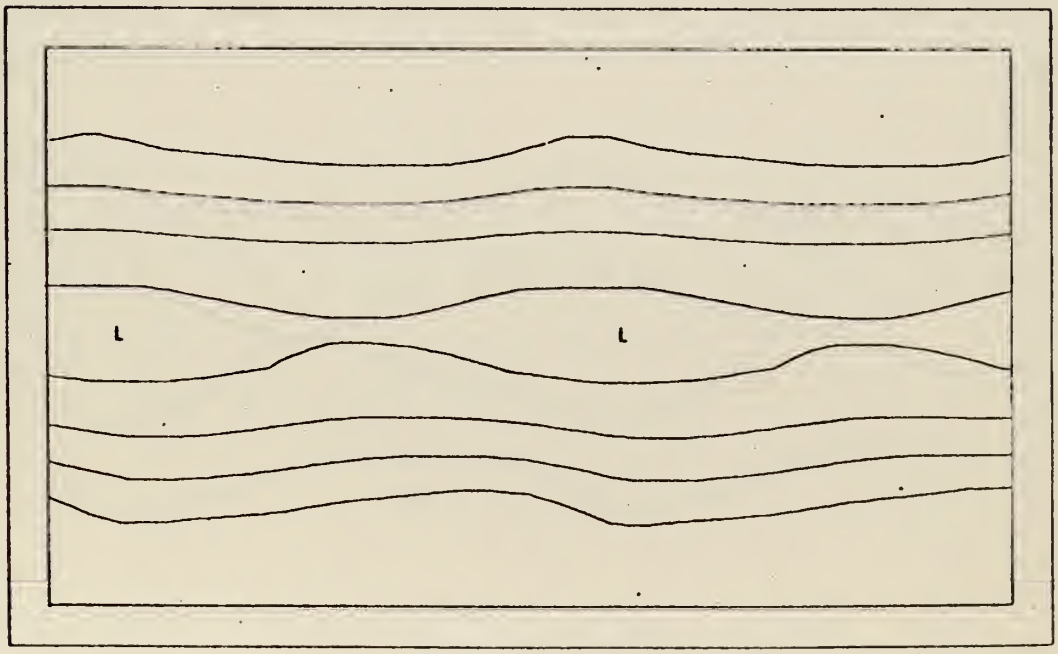

Figure 25. Stream function field at 15 days for A=constant form of dissipation

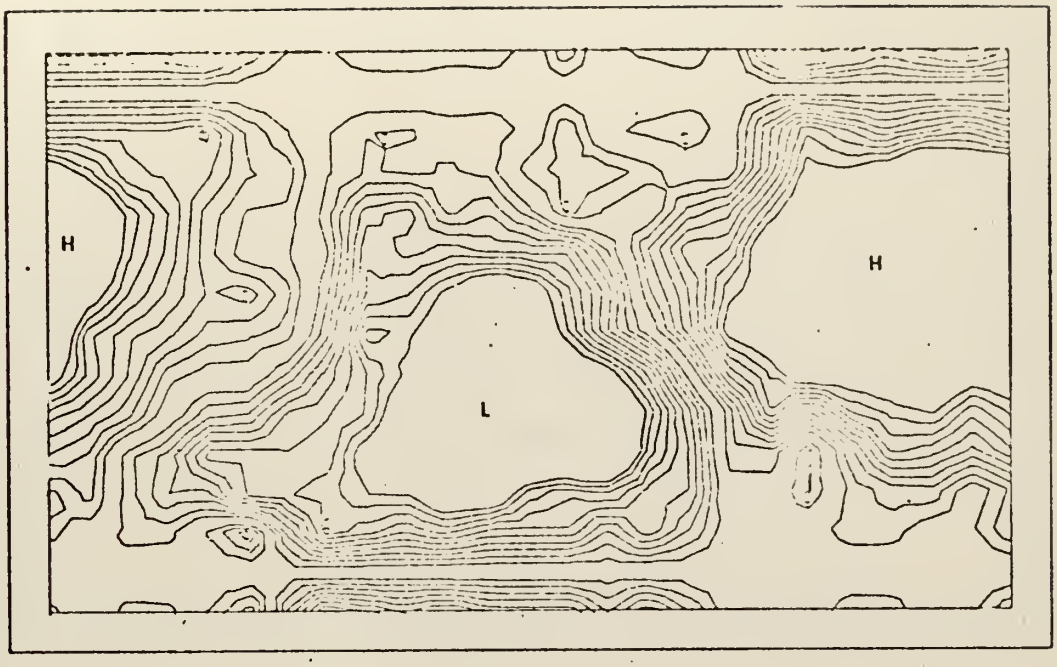

Figure 26. Stream function field at 20 days for zero forcing and zero dissipation case

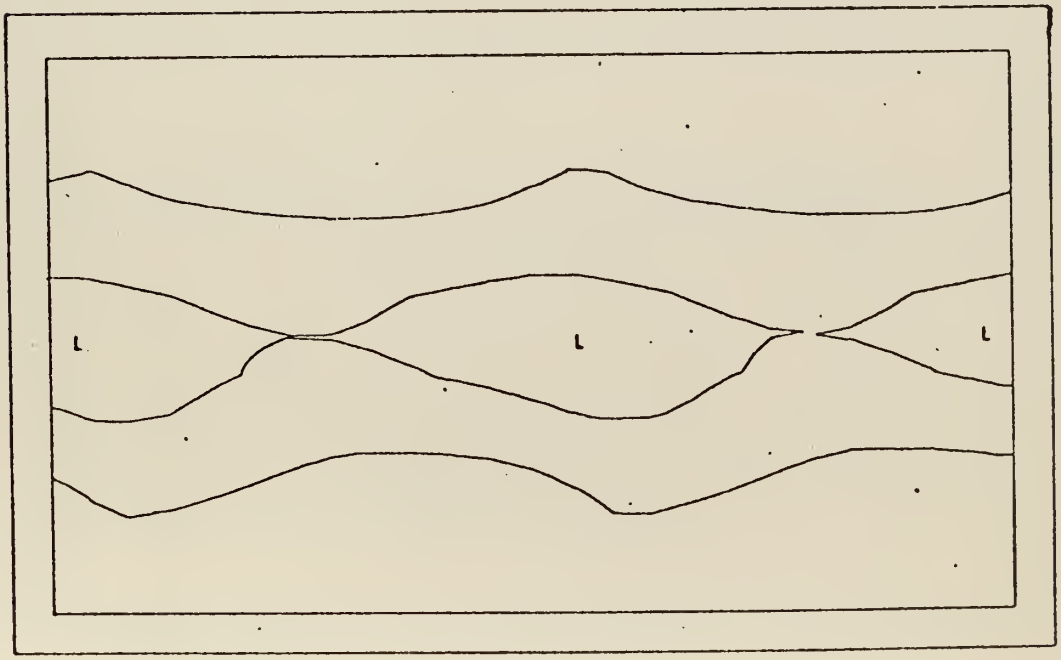

Figure 27. Stream function field at 20 days for A=constant form of dissipation

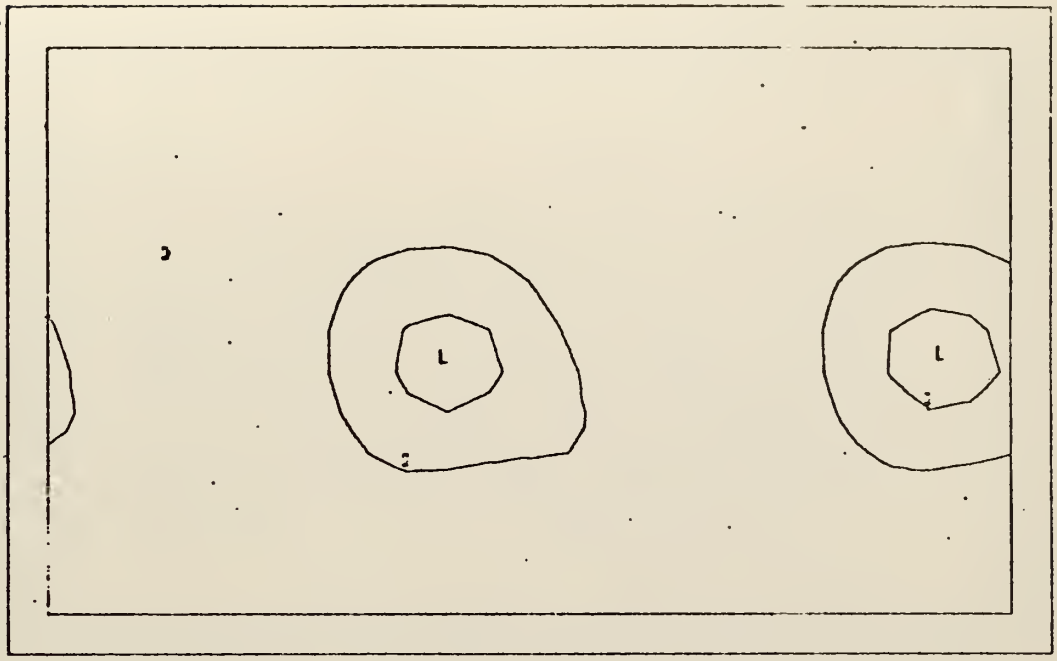

Figure 28. Stream function field at 5 days for A_L form of dissipation with gamma=.5

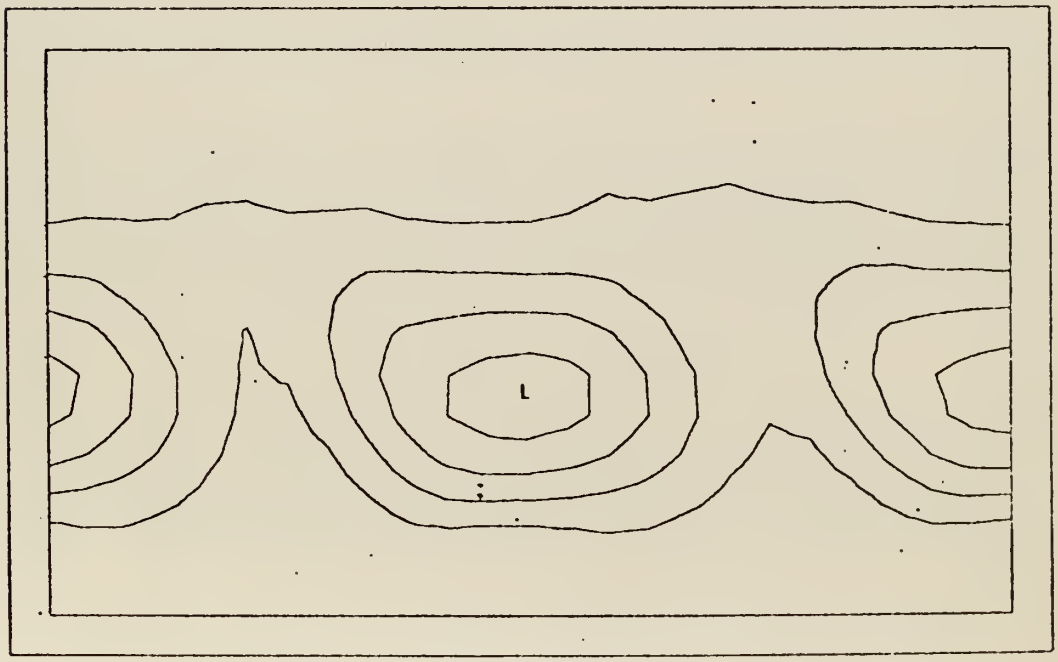

Figure 29. Stream function field at 5 days for A_L form of dissipation with gamma=.2

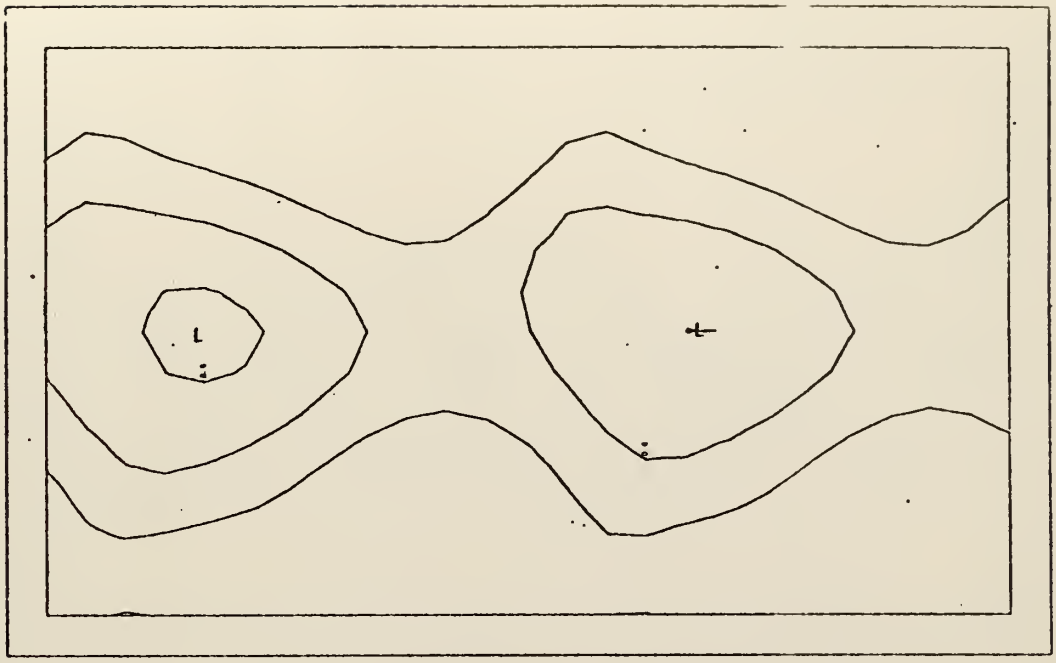

Figure 30. Stream function field at 10 days for A_L form of dissipation with gamma=.5

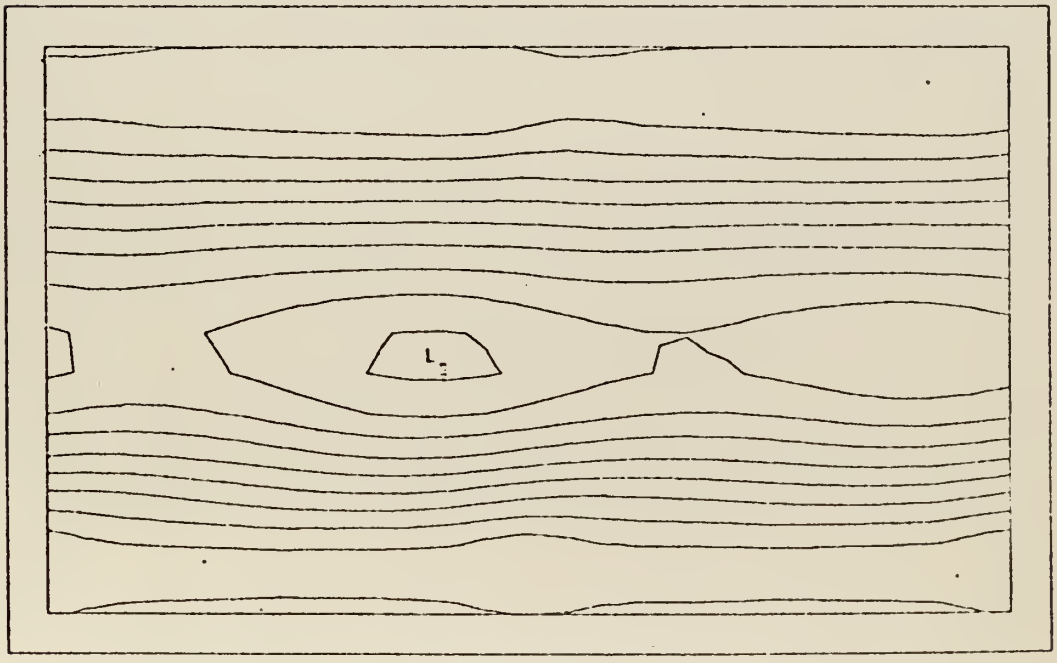

Figure 31. Stream function field at 10 days for A_L form of dissipation with gamma=.2

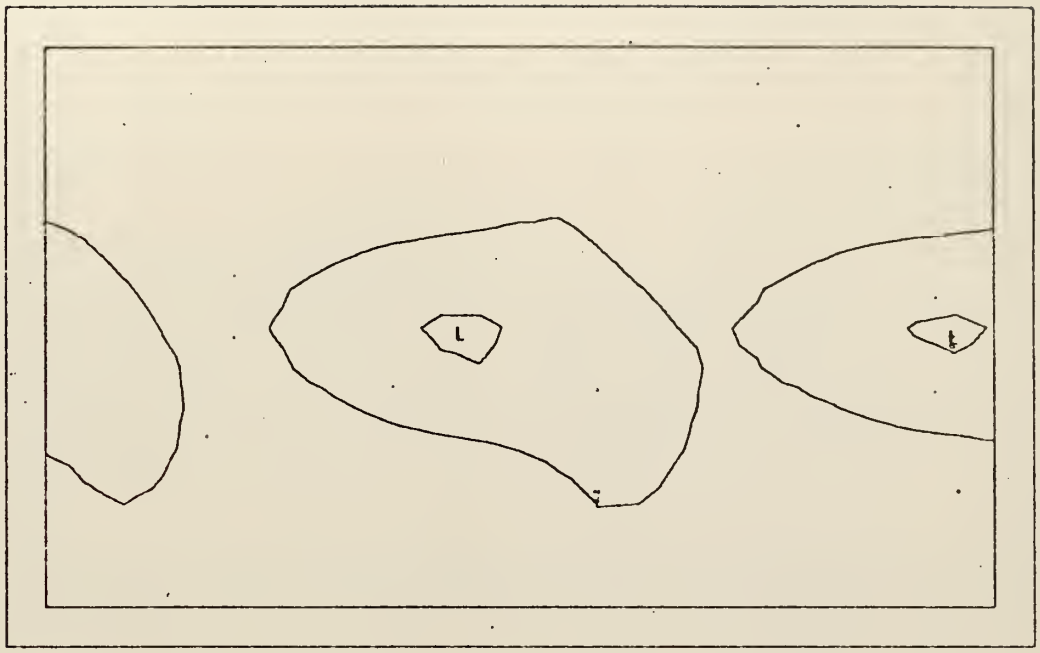

Figure 32. Stream function field at 15 days for A_L form of dissipation with gamma=.5

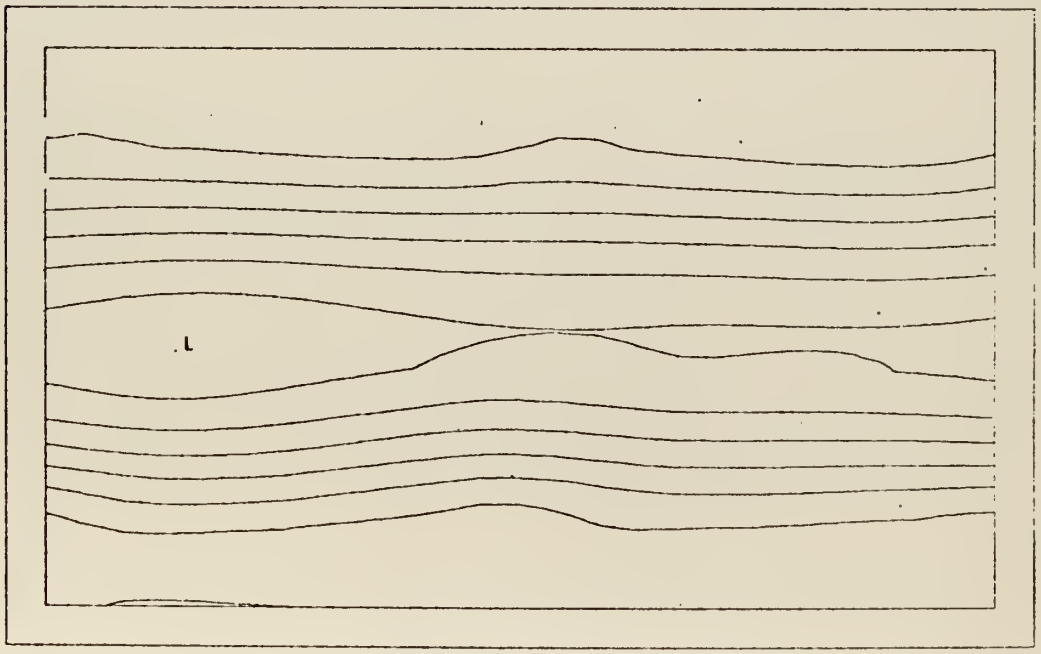

Figure 33. Stream function field at 15 days for A_L form of dissipation with gamma=.2

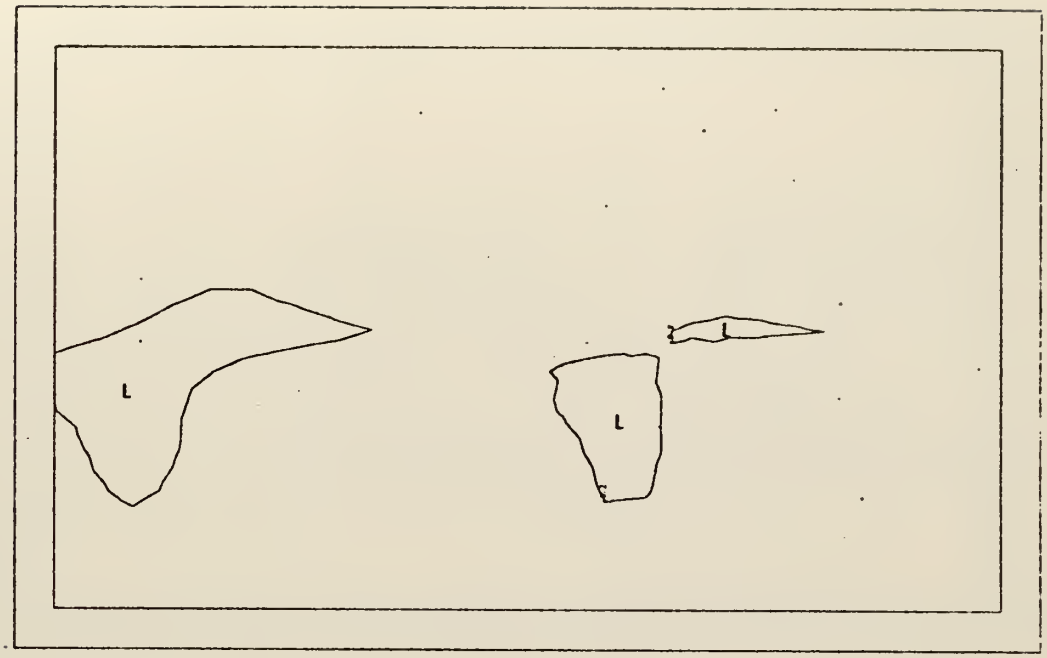

Figure 34. Stream function field at 20 days for A_L form of dissipation with gamma=.5

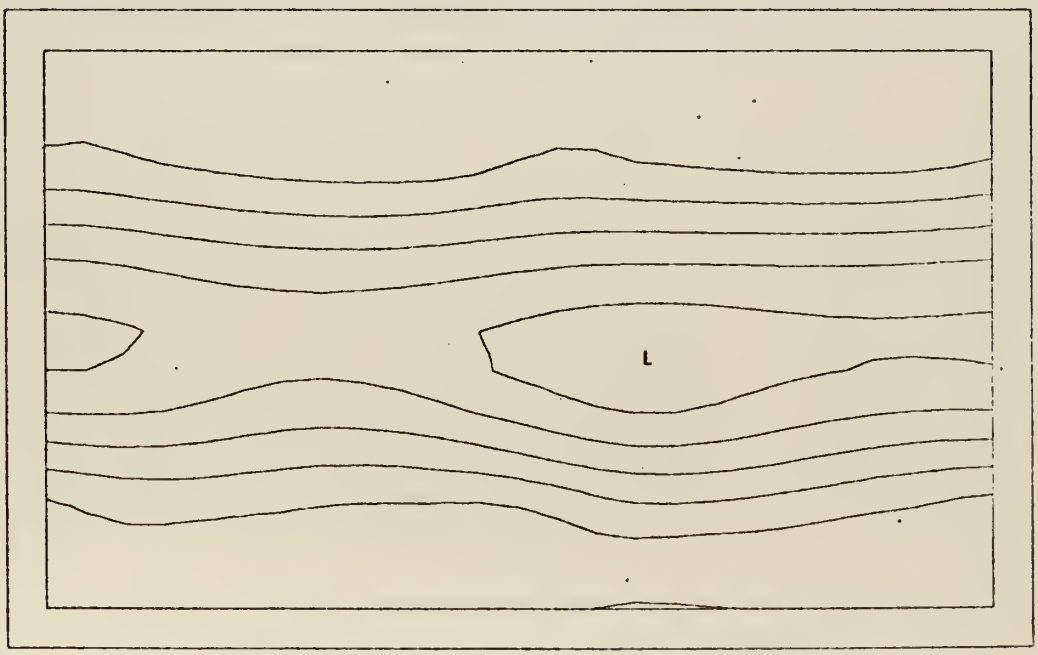

Figure 35. Stream function field at 20 days for A_L form of dissipation with gamma=.2

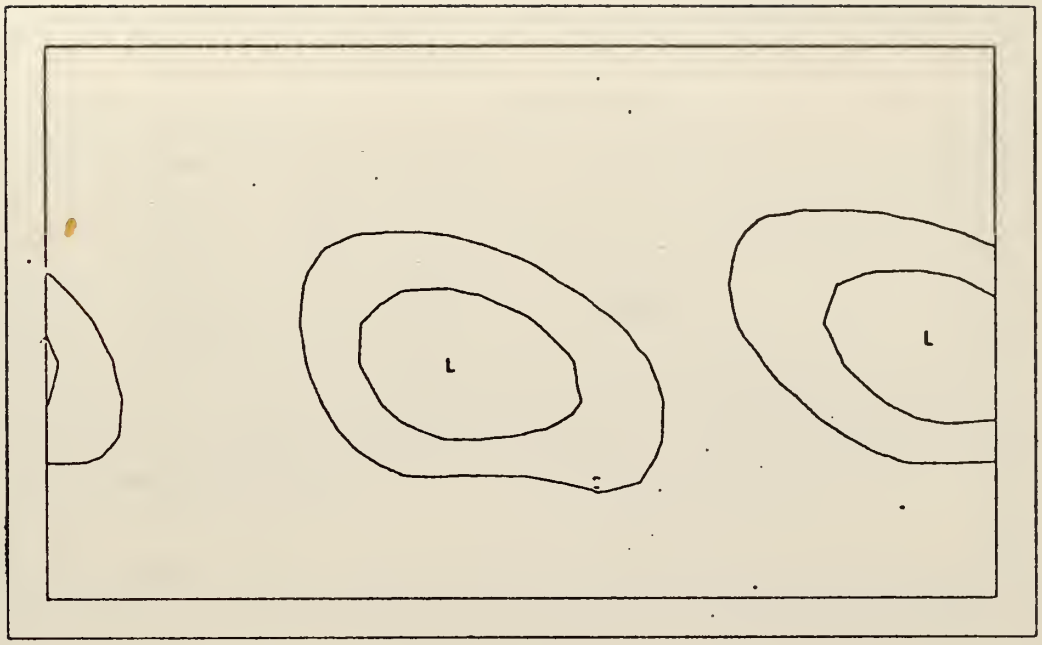

Figure 36. Stream function field at 5 days for A_S form of dissipation with gamma=.5

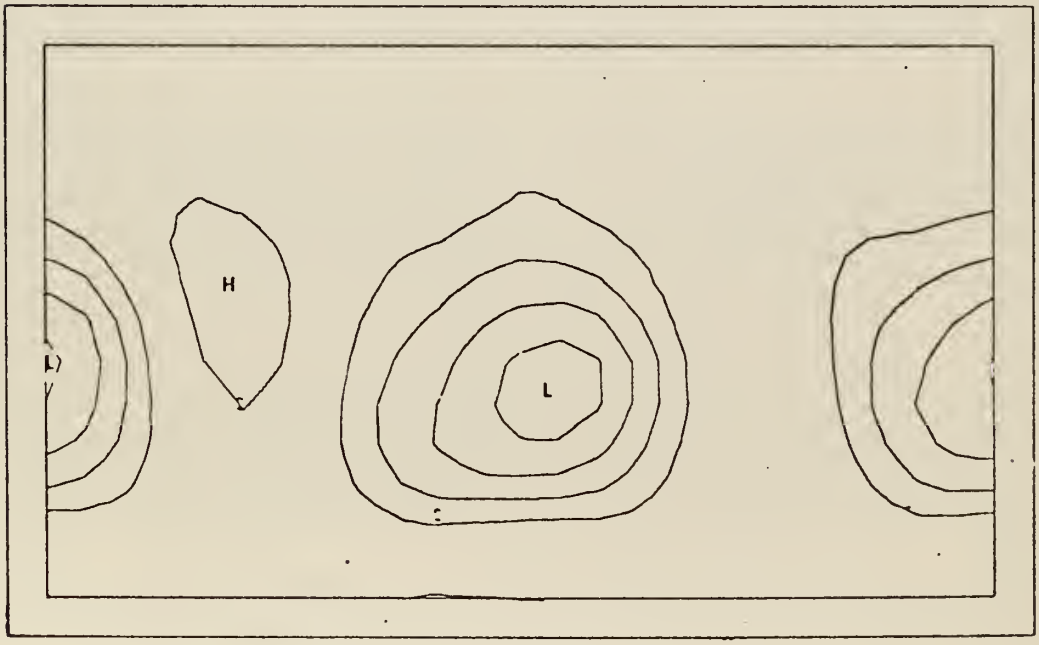

Figure 37. Stream function field at 5 days for A_S form of dissipation with gamma=.2

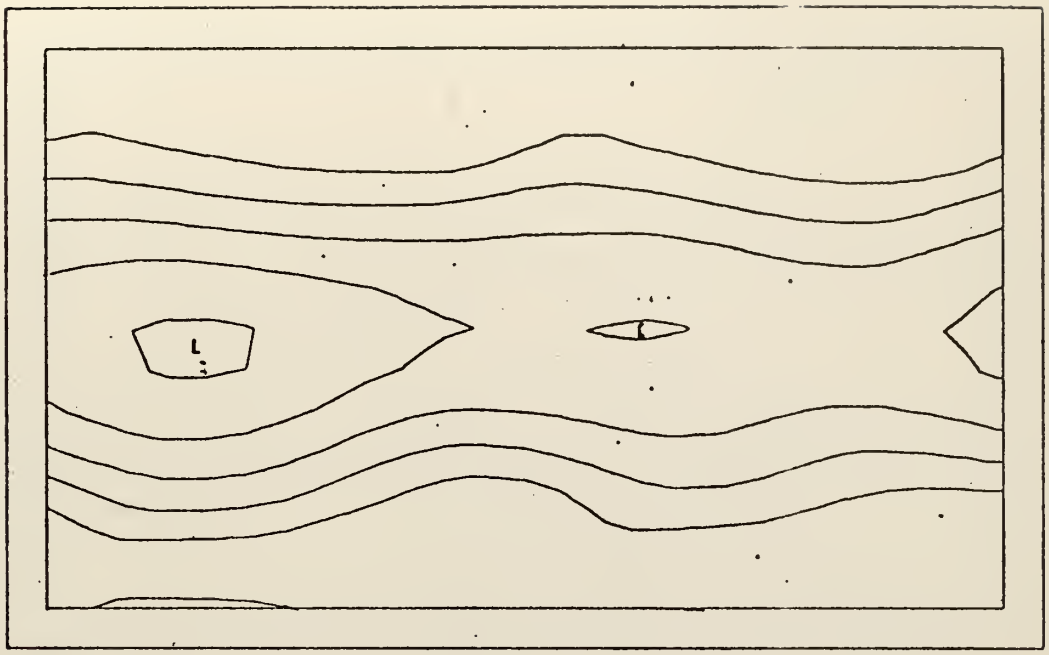

Figure 38. Stream function field at 10 days for A_s form of dissipation with gamma=.5

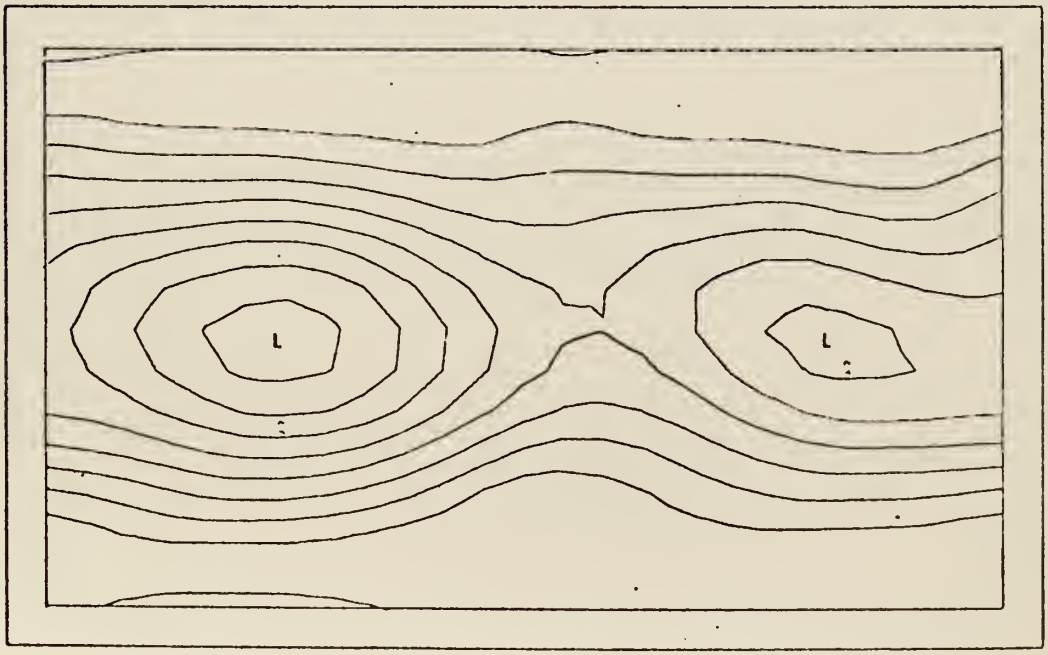

Figure 39. Stream function field at 10 days for A_s form of dissipation with gamma=.2

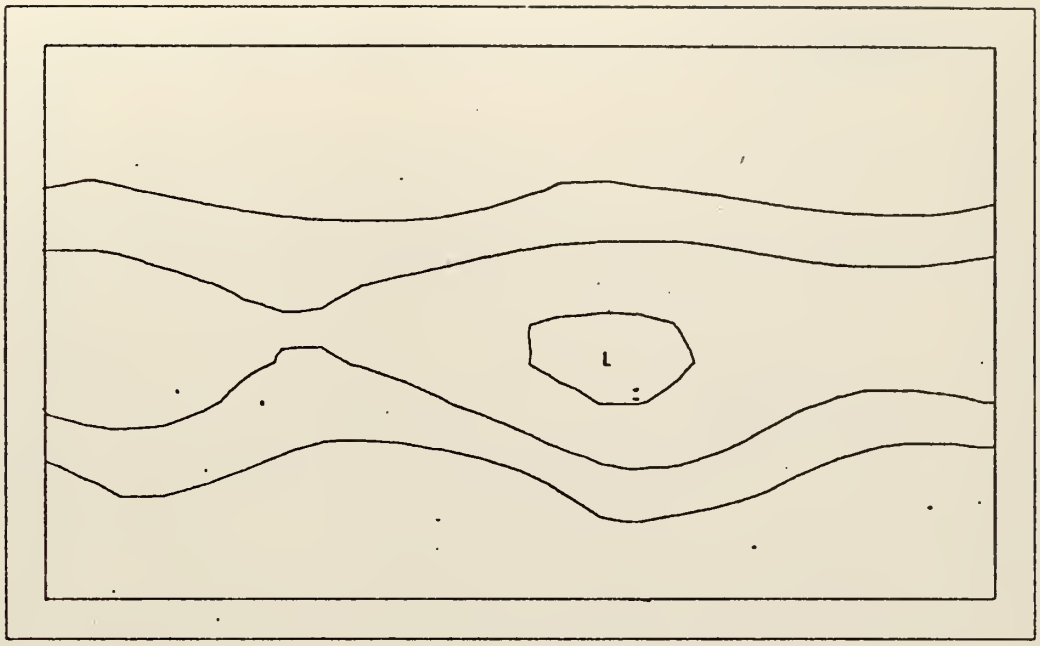

Figure 40. Stream function field at 15 days for A_s form of dissipation with gamma=.5

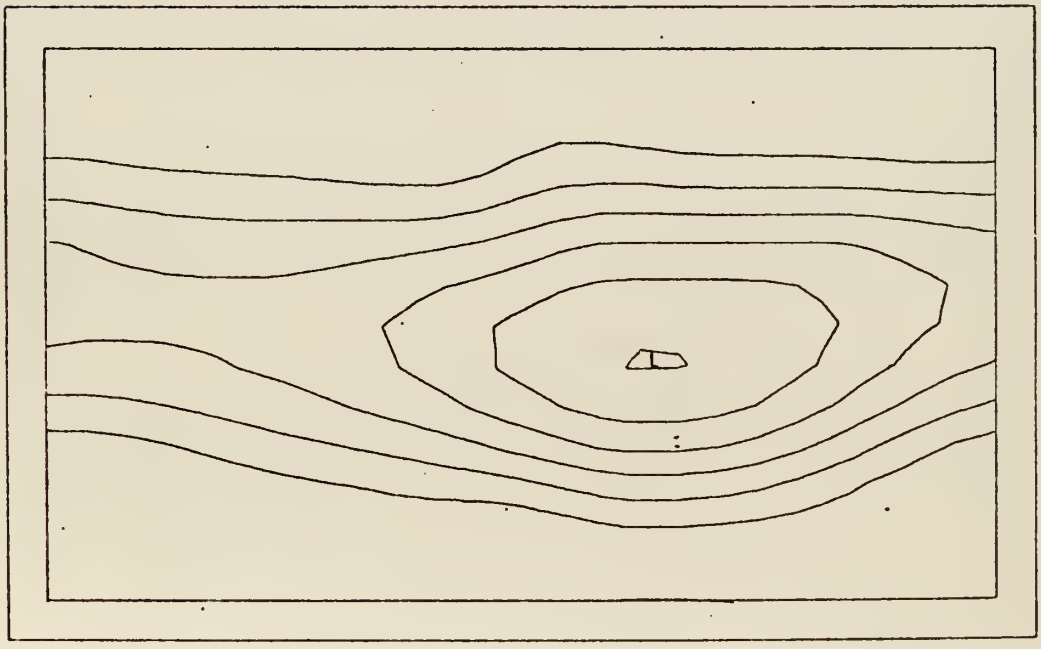

Figure 41. Stream function field at 15 days for A_s form of dissipation with gamma=.2

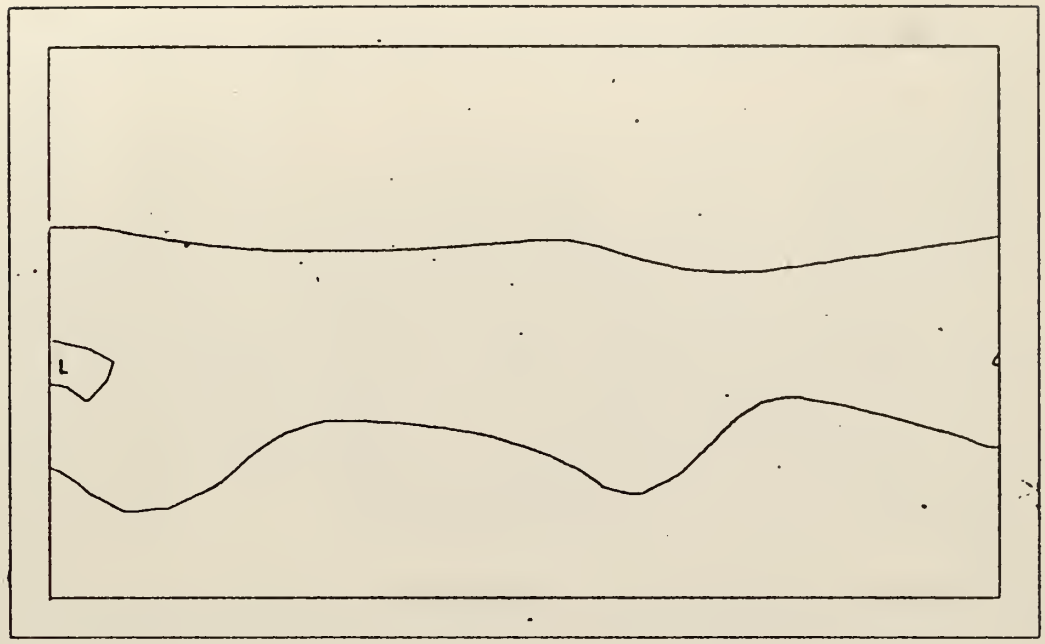

Figure 42. Stream function field at 20 days for A_s form of dissipation with gamma=.5

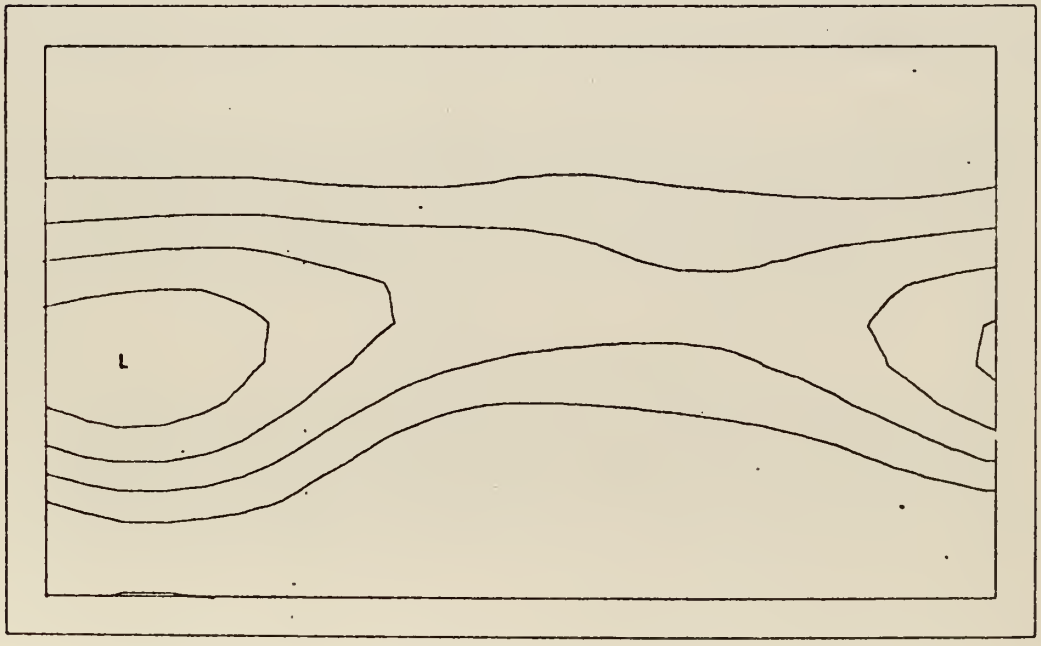

Figure 43. Stream function field at 20 days for A_s form of dissipation with gamma=.2

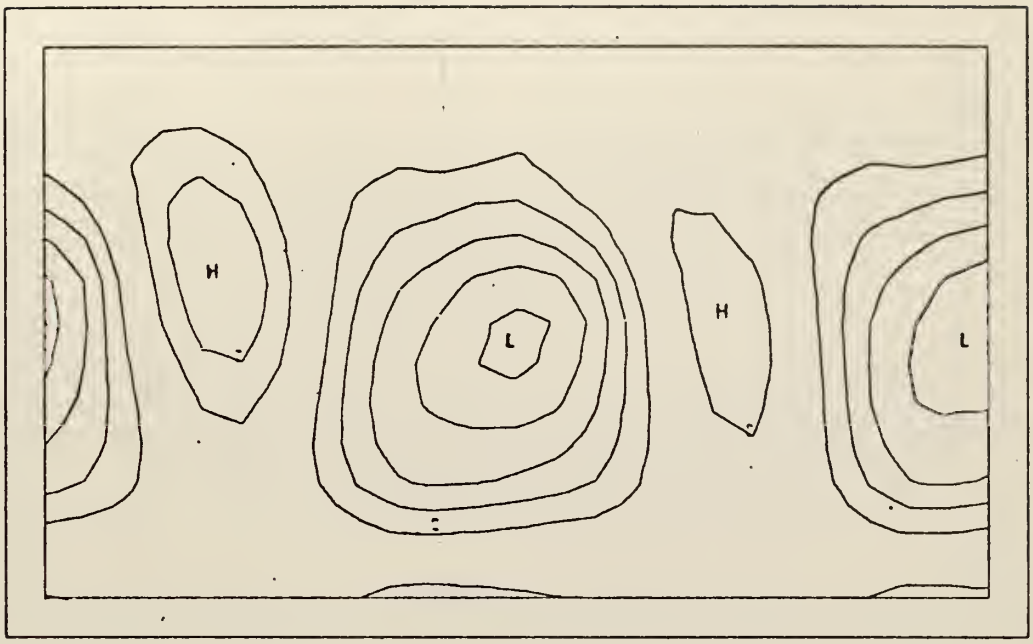

Figure 44. Stream function field at 5 days for A_S form of dissipation with gamma=.13

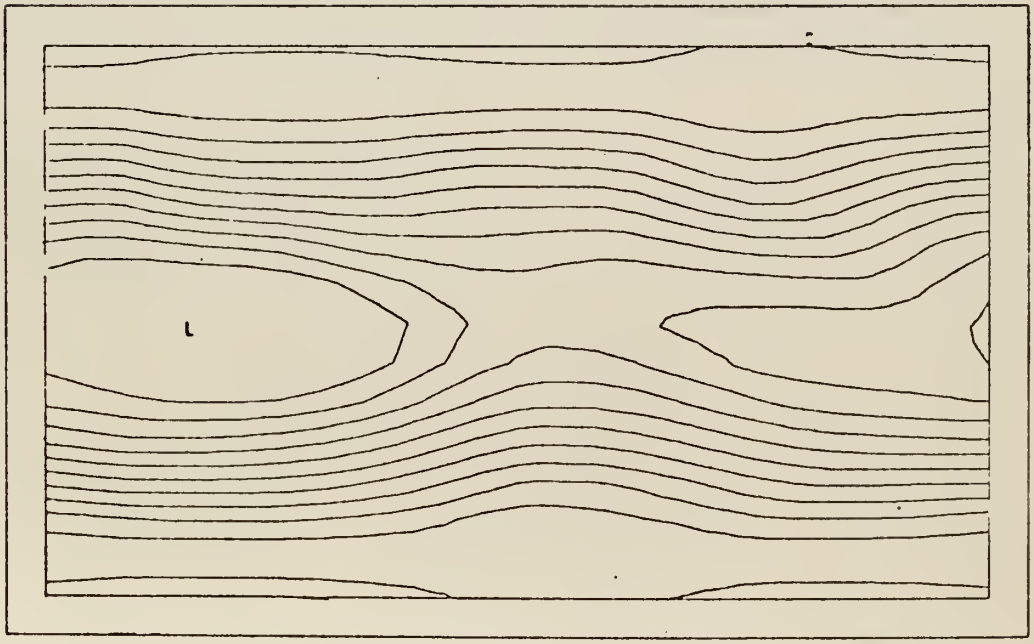

Figure 45. Stream function field at 10 days for A_S form of dissipation with gamma=.13

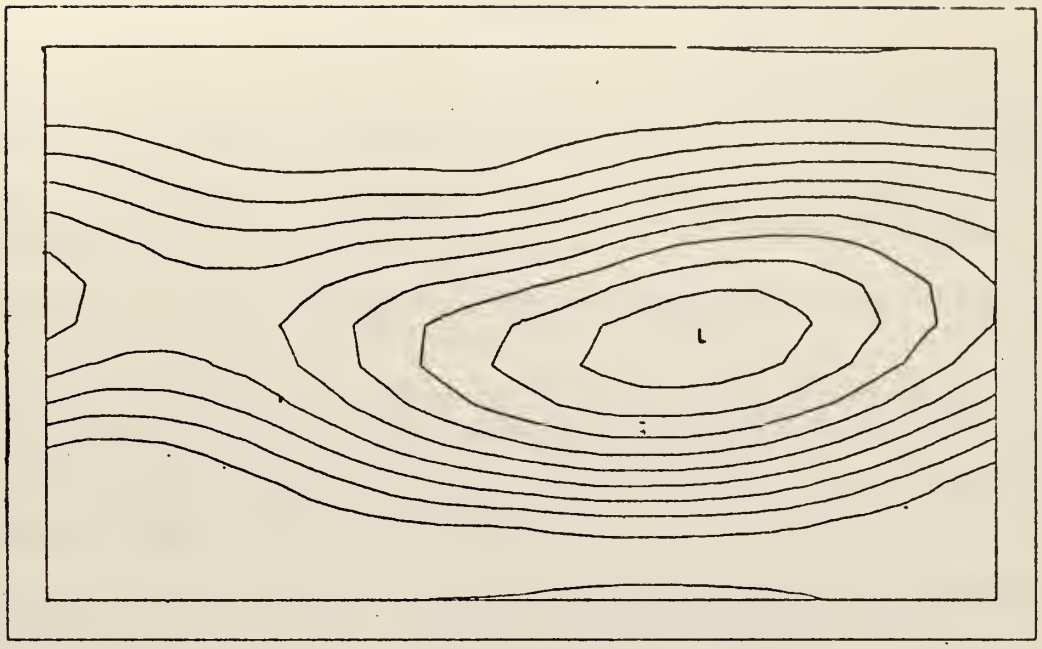

Figure 46. Stream function field at 15 days for A_s form of dissipation with gamma=.13

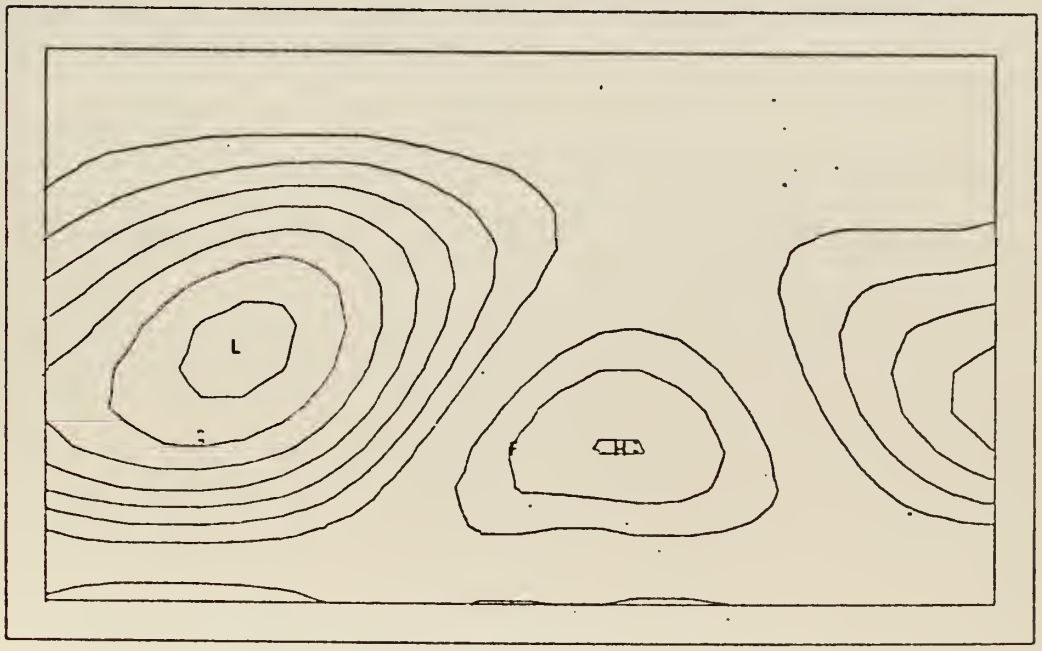

Figure 47. Stream function field at 20 days for A_s form of dissipation with gamma=.13

LIST OF REFERENCES

1. Deardoff, J. W., 1971: On the magnitude of the subgrid scale eddy coefficient. Journal of Computational Physics, Vol. 7, No. 1, 120-133.

2. Haltiner, G. J. and F. L. Martin, 1957: Dynamical and Physical Meteorology. McGraw-Hill Book Company, New York, Toronto, London.

3. Haltiner, G. J., 1971: Numerical Weather Prediction. John Wiley and Sons, Inc., New York, London, Sydney, Toronto.

4. Leith, C. E., 1968: Two dimensional eddy viscosity coefficients. Technical Report of the Japan Meteorological Agency, No. 67, I-41 - I-44.

5. Lily, D. K., 1969: Numerical simulation of two dimensional turbulence. Physics of Fluids, Suppl II, 240-249.

6. Lily, D. K., 1971: Numerical simulation of developing and decaying two-dimensional turbulence. Journal of Fluid Mechanics, Vol. 45, Part 2, 395-415.

7. Lily, D. K., 1972: Numerical simulation studies of two-dimensional turbulence. Geophysical Fluid Dynamics, Vol. 3, 289-319.

8. Smagorinsky, J., 1963: General circulation experiments with the primitive equations. Monthly Weather Review, Vol. 91, No. 3, 99-154.

9. Smagorinsky, J., Circa 1960: The formulation of eddy transport processes for the quasi-static inertial subrange of atmospheric motions. Unpublished manuscript.

INITIAL DISTRIBUTION LIST

		No. Copies
1.	Defense Documentation Center Cameron Station Alexandria, Virginia 22314	2
2.	Library, Code 0212 Naval Postgraduate School Monterey, California 93940	2
3.	Dr. George J. Haltiner Chairman, Department of Meteorology Naval Postgraduate School Monterey, California 93940	5
4.	Dr. W. L. Gates The Rand Corporation 1700 Main Street Santa Monica, California 90406	5
5.	Lieutenant Orlin R. Scrivener, USN U. S. Fleet Weather Central COMNAVMARIANAS, Box 12 FPO San Francisco, California 96630	5
6.	Naval Weather Service Command Washington Navy Yard Washington, D. C. 20390	1
7.	Commanding Officer Fleet Numerical Weather Central Naval Postgraduate School Monterey, California 93940	1
8.	Commanding Officer Environmental Prediction Research Facility Naval Postgraduate School Monterey, California 93940	1
9.	Department of Meteorology, Code 51 Naval Postgraduate School Monterey, California 93940	3
10.	Department of Oceanography, Code 58 Naval Postgraduate School Monterey, California 93940	1

11. Dr. R. T. Williams, Code 51Wu — 1
Department of Meteorology
Naval Postgraduate School
Monterey, California 93940

12. Dr. R. L. Haney, Code 51Hy — 1
Department of Meteorology
Naval Postgraduate School
Monterey, California 93940

13. Dr. J. Smagorinsky — 1
Director
Geophysical Fluid Dynamics Laboratory
Princeton University
Princeton, New Jersey 08540

14. Dr. C. E. Leith — 1
National Center for Atmospheric Research
Box 1470
Boulder, Colorado 80302

15. Dr. D. K. Lily — 1
National Center for Atmospheric Research
Box 1470
Boulder, Colorado 80302

16. Dr. A. Arakawa — 1
Department of Meteorology
U.C.L.A.
Los Angeles, California 90024

17. Dr. R. L. Elsberry, Code 51Es — 1
Department of Meteorology
Naval Postgraduate School
Monterey, California 93940

Security Classification

DOCUMENT CONTROL DATA - R & D

(Security classification of title, body of abstract and indexing annotation must be entered when the overall report is classified)

1. ORIGINATING ACTIVITY *(Corporate author)*

Naval Postgraduate School
Monterey, California 93940

2a. REPORT SECURITY CLASSIFICATION

Unclassified

2b. GROUP

3. REPORT TITLE

The Form of Lateral Viscosity in Atmospheric Flows

4. DESCRIPTIVE NOTES *(Type of report and inclusive dates)*

Master's Thesis; September 1972

5. AUTHOR(S) *(First name, middle initial, last name)*

Orlin R. Scrivener

6. REPORT DATE	7a. TOTAL NO. OF PAGES	7b. NO. OF REFS
	66	9

8a. CONTRACT OR GRANT NO.	9a. ORIGINATOR'S REPORT NUMBER(S)
b. PROJECT NO.	
c.	9b. OTHER REPORT NO(S) *(Any other numbers that may be assigned this report)*
d.	

10. DISTRIBUTION STATEMENT

Approved for public release; distribution unlimited.

11. SUPPLEMENTARY NOTES	12. SPONSORING MILITARY ACTIVITY
	Naval Postgraduate School Monterey, California 93940

13. ABSTRACT

Long term numerical integrations were performed on a two-dimensional model utilizing the barotropic vorticity equation including a space- and time-dependent forcing function and a laminar-type viscosity term. Three different forms of the laminar type viscosity or dissipation term were used. A comparison was made of the effects these different dissipation terms had on the time-dependence of total kinetic energy, total enstrophy, and total gradient of vorticity squared, the spectral distribution of kinetic energy and enstrophy, and the stream function field. A difference of behavior of all the above variables was found for each form of dissipation.

DD FORM 1 NOV 65 1473 (PAGE 1)

S/N 0101-807-6811

Security Classification

A-31408

14 KEY WORDS	LINK A		LINK B		LINK C	
	ROLE	WT	ROLE	WT	ROLE	WT
Lateral viscosity						
Dissipation						
Turbulence						
"Eddy Diffusion"						

DD FORM 1 NOV 68 1473 (BACK)

S/N 0101-807-6821

133010

Thesis
S4035
c.1

Scrivener
The form of lateral viscosity in atmospheric flows.